SUPPORTING INFORMATION

Targeting mPGES-1 by a combinatorial approach: identification of the aminobenzothiazole scaffold to suppress PGE_2 levels

Maria G. Chini,[†, ⊥, ∇] Assunta Giordano,[†, ‡, ∇] Marianna Potenza,[†] Stefania Terracciano,[†] Katrin Fischer,[§] Maria C. Vaccaro,[†] Ester Colarusso,[†] Ines Bruno,[†] Raffaele Riccio,[†] Andreas Koeberle,[§, ¶] Oliver Werz,[§] and Giuseppe Bifulco[†,*]

[†]Department of Pharmacy, University of Salerno, via Giovanni Paolo II, 132, 84084, Fisciano, Italy. E-mail: bifulco@unisa.it.

[⊥]Department of Biosciences and Territory, University of Molise, Contrada Fonte Lappone, Pesche, Isernia, I-86090, Italy.

[‡]Institute of Biomolecular Chemistry (ICB), Consiglio Nazionale delle Ricerche (CNR), Via Campi Flegrei 34, I-80078, Pozzuoli, Napoli, Italy.

[§]Department of Pharmaceutical/Medicinal Chemistry, Institute of Pharmacy, Friedrich Schiller University Jena, Jena, Germany.

[¶]Michael Popp Research Institute, University of Innsbruck, Innsbruck, Austria.

TABLE OF CONTENTS

Computational details

Schrödinger suite[1] was used for the preparation of the combinatorial libraries and the successive phase of the Virtual Screening Protocol.

The structures of the reagents, namely all commercially available acyl chlorides and boronates at Sigma Aldrich Company, were converted from 2D structures to all-atom 3D structures suitable for the docking stage of the process, using Reagent Preparation software.[2] The .bld file obtained from this process were combined with the synthones 2-amino-6- (**A**) and 2-amino-5-bromobenzothiazole (**B**), by Combiglide software,[3] obtaining 180,120 molecules for each library. For each combinatorial library, all tautomers and ionization states at pH of 7.4 ± 1 were considered by the LigPrep program,[4] obtaining two large libraries of and of 212,126 for 2-amino-6-bromobenzothiazole (**A**) and for 212,097 for 2-amino-5-bromobenzothiazole (**B**) molecules. The successive application of LigFilter software,[4] the number of molecules was reduced to 31,240 for the scaffold **A** and to 31,341 for the scaffold **B**, considering the pharmacokinetic properties calculated by QikProp software,[5] which were submitted to the successive structure-based virtual screening workflow.[6] After the application of Virtual Screening Workflow,[6] 2,949 molecules for the scaffold **A** and 2821 for the scaffold **B** were obtained; afterwards, considering a docking energy cut-off of -7.0 kcal/mol, only 137 for the first one and 190 for the second one were submitted to the successive detailed computational analysis. Then, the most promising 13 molecules (**1**-**13**) were suggested for the synthesis, after the evaluation of PAINS (*vide infra*).

The protocol employed for the identification of novel mPGES-1 inhibitors involved structure-based computational methodologies. mPGES-1 crystal structure (PDB code: 4BPM)[7] was used for the structure-based molecular docking experiments (3D-protein structure). Protein 3D model was prepared using the Schrödinger Protein Preparation Wizard,[8] starting from the mPGES-1 X-ray structure in the active form co-complexed with the inhibitor LVJ (2-[[2,6-bis(chloranyl)-3-[(2,2-dimethylpropanoylamino)methyl]phenyl]amino]-1-methyl-6-(2-methyl-2-oxidanyl-propoxy)-N-

[2,2,2-tris(fluoranyl)ethyl]benzimidazole-5-carboxamide) (PDB code: 4BPM).[7] During the molecular docking calculation, the receptor grid generated focused onto the co-crystallized ligand-binding site (LVJ) was used, with inner- and outer-box dimensions of 18×18×18 Å and 34.7×34.7×34.7 Å, respectively.

Structure-based molecular docking experiments were performed using the combinatorial libraries of compounds and the mPGES-1 3D protein structure,

The Virtual Screening was performed using the Virtual Screening Workflow as implemented in Schrödinger Suite and using Glide software [9-12] following the:

- High-Throughput Virtual Screening scoring and sampling (HTVS) (input: 31,240 for the scaffold **A** and to 31,341 for the scaffold **B**), saved first 40% of ranked compounds
- Standard Precision scoring and sampling phase (SP), saved the first 40% of ranked compounds
- Extra Precision scoring and sampling phase (XP), saved first 60% of ranked compounds as the final output

In order to assess the reliability of the mPGES-1 system for docking experiments, we have compared two mPGES-1 structures co-crystallized with inhibitors, mentioned in the main text, acting as substrate (PGH_2) competitors (PDB codes: 4BPM, 4YLK5) with the predicted docking complexes. Specifically, the latters were computed *in silico* between the specific mPGES-1 protein structure used in this study (PDB code: 4BPM) and the two inhibitors.

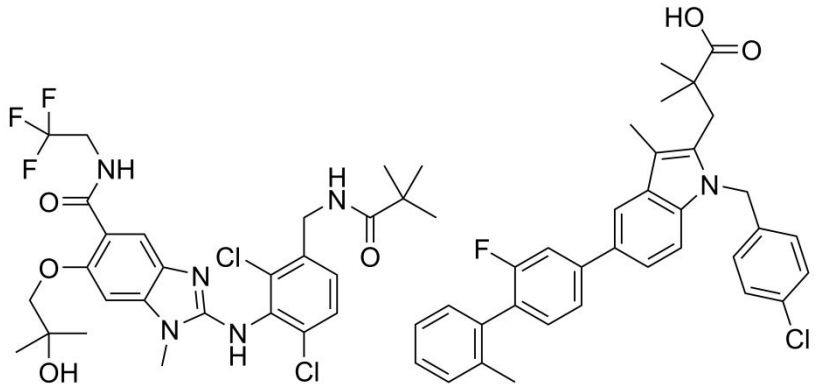

4BPM_inhibitor (LVJ) **4YK5_inhibitor**

Figure S 1. Chemical structures of co-crystallized mPGES-1 inhibitors acting as substrate (PGH_2) competitors (PDB codes: 4BPM, 4YLK5).

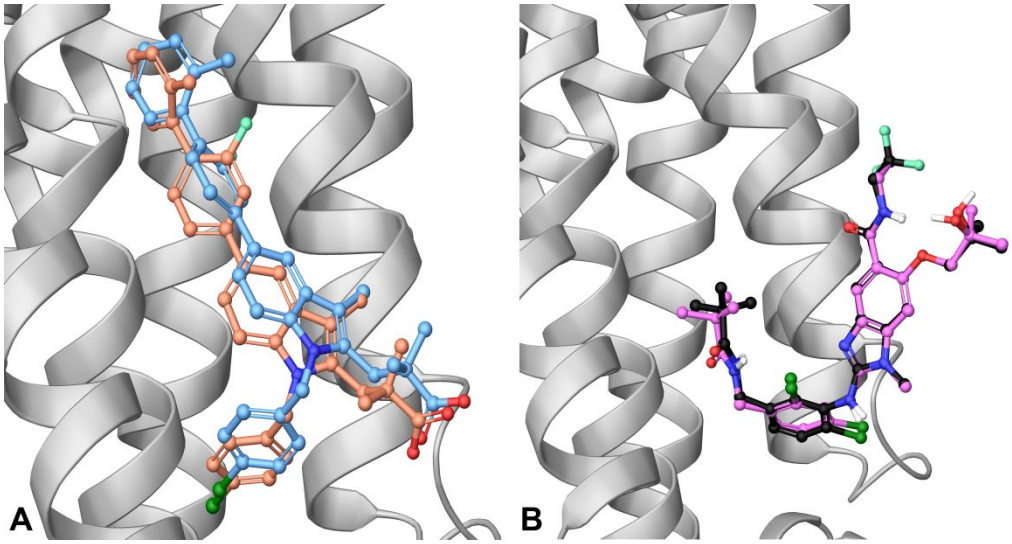

Figure S 2. Comparison between the experimental and calculated binding mode of the mPGES-1 co-crystallized inhibitors, acting as substrate competitors.
The latters using the mPGES-1 protein structure used in this study, and deposited in the Protein Data Bank with the code: 4BPM.
Panel A) 3D representation of the superimposition between experimental (cyan sticks) and calculated (salmon pink sticks) binding mode of the mPGES-1 co-crystallized ligand related to 4YK5 pdb code. The calculated binding mode of co-crystallized ligand related to 4YK5 pdb code provided a predicted energy of binding = -8.1 kcal mol^{-1}.
Panel B) 3D representation of the superimposition between experimental (black sticks) and calculated (fuchsia sticks) binding mode of the mPGES-1 co-crystallized ligand related to 4BPM pdb. The calculated binding mode of co-crystallized ligand related to 4BPM pdb code provided a predicted energy of binding = -8.3 kcal mol^{-1}

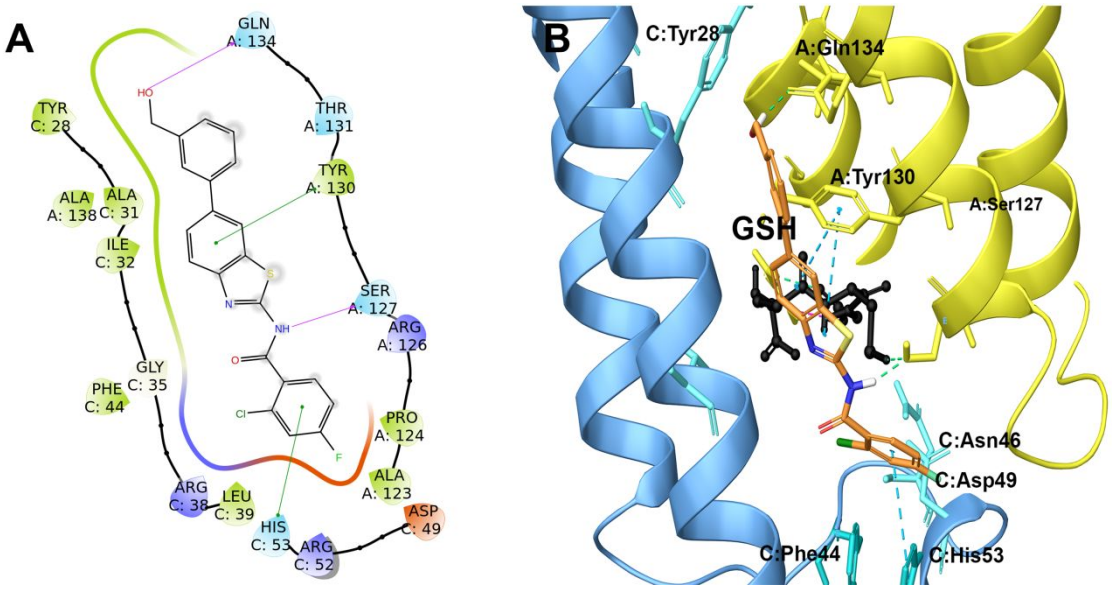

Figure S 3. 2D and 3D representation of the interaction pattern between **1** and mPGES-1.
Panel A) 2D interactions diagram of compound **1** with mPGES-1 receptor counterpart (pdb code: 4BPM); h-bond interactions are reported as purple arrows, while π-π interactions as green lines; GSH is depicted in grey, hydrophobic residues in green, and positive and negative charged residues in blue and red respectively. **Panel B)** 3D representation of compound **1** (light orange sticks) in the binding site of mPGES-1 (pdb code: 4BPM). mPGES-1 chain A and its key residues are depicted in yellow ribbons and stick, mPGES-1 chain C and its key residues are in cyan ribbons and stick, GSH is reported as black sticks and balls. All the interactions are represented as dotted lines, green for hydrogen bonds, cyano for π-π interactions, violet for halogen bonds.
The calculated binding mode of **2** provided a predicted energy of binding = -8.0 kcal mol^{-1}.

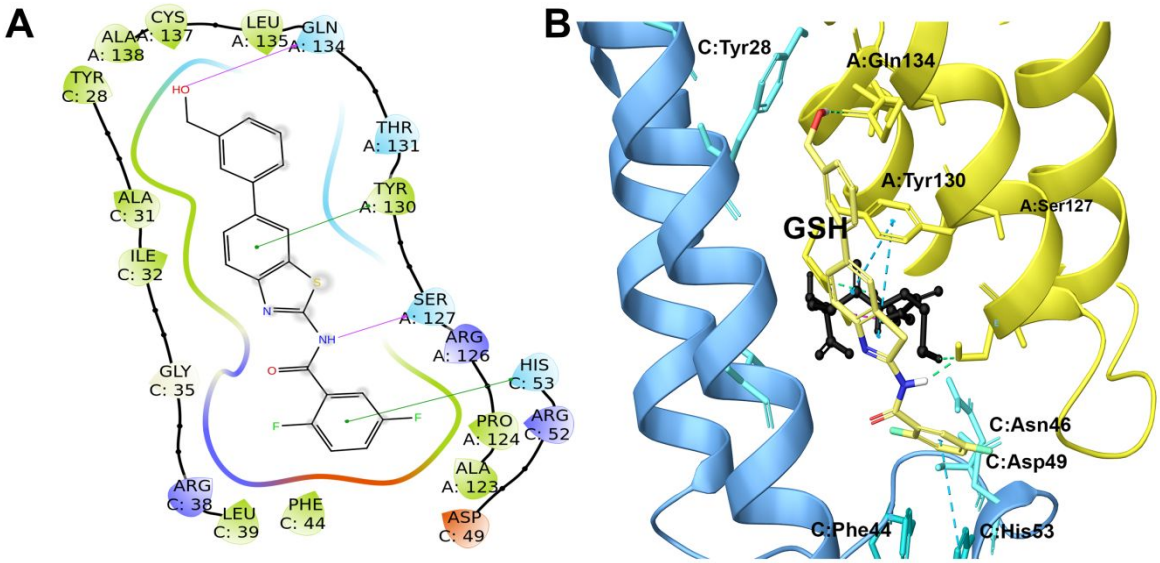

Figure S 4. 2D and 3D representation of the interaction pattern between **2** and mPGES-1.
Panel A) 2D interactions diagram of compound **2** with mPGES-1 receptor counterpart (pdb code: 4BPM); h-bond interactions are reported as purple arrows, while π-π interactions as green lines; GSH is depicted in grey, hydrophobic residues in green, and positive and negative charged residues in blue and red respectively. **Panel B)** 3D representation of compound **2** (yellow sticks) in the binding site of mPGES-1 (pdb code: 4BPM). mPGES-1 chain A and its key residues are depicted in yellow ribbons and stick, mPGES-1 chain C and its key residues are in cyan ribbons and stick, GSH

is reported as black sticks and balls. All the interactions are represented as dotted lines, green for hydrogen bonds, cyano for π-π interactions, violet for halogen bonds.
The calculated binding mode of **2** provided a predicted energy of binding = -7.9 kcal mol^{-1}.

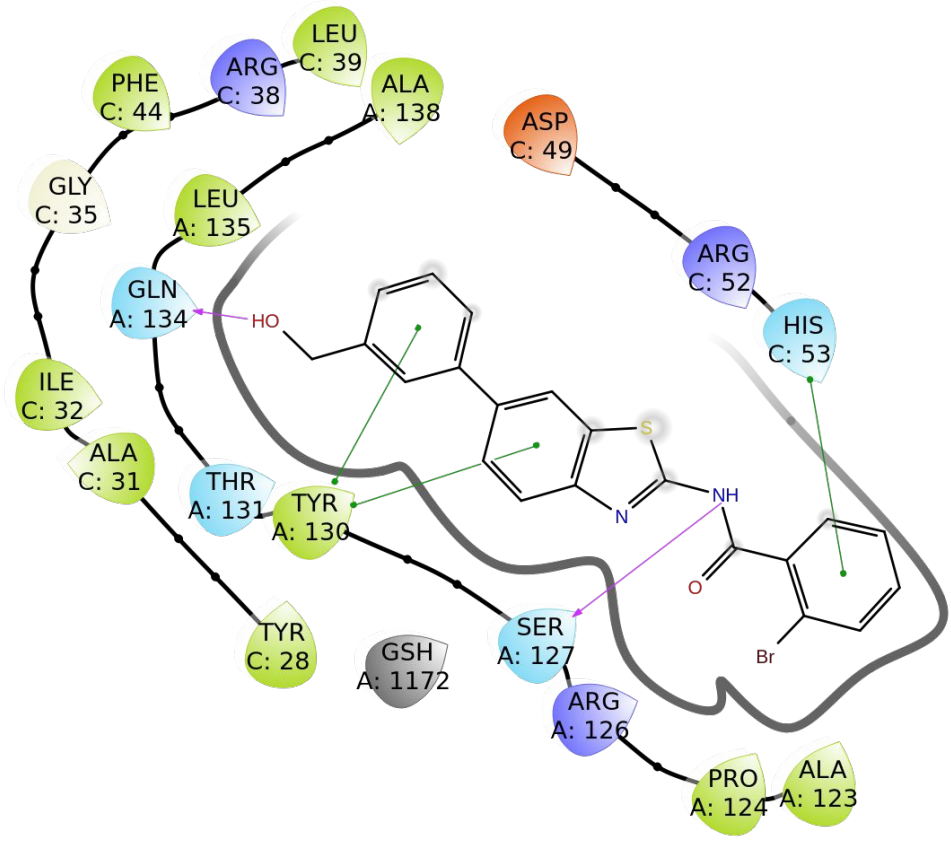

Figure S 5. 2D representation of the interaction pattern between **3** and mPGES-1.
Panel A) 2D interactions diagram of compound **3** with mPGES-1 receptor counterpart (pdb code: 4BPM); h-bond interactions are reported as purple arrows, while π-π interactions as green lines; GSH is depicted in grey, hydrophobic residues in green, and positive and negative charged residues in blue and red respectively. All the interactions are represented as dotted lines, green for hydrogen bonds, cyano for π-π interactions, violet for halogen bonds.
The calculated binding mode of **3** provided a predicted energy of binding = -7.7 kcal mol^{-1}.

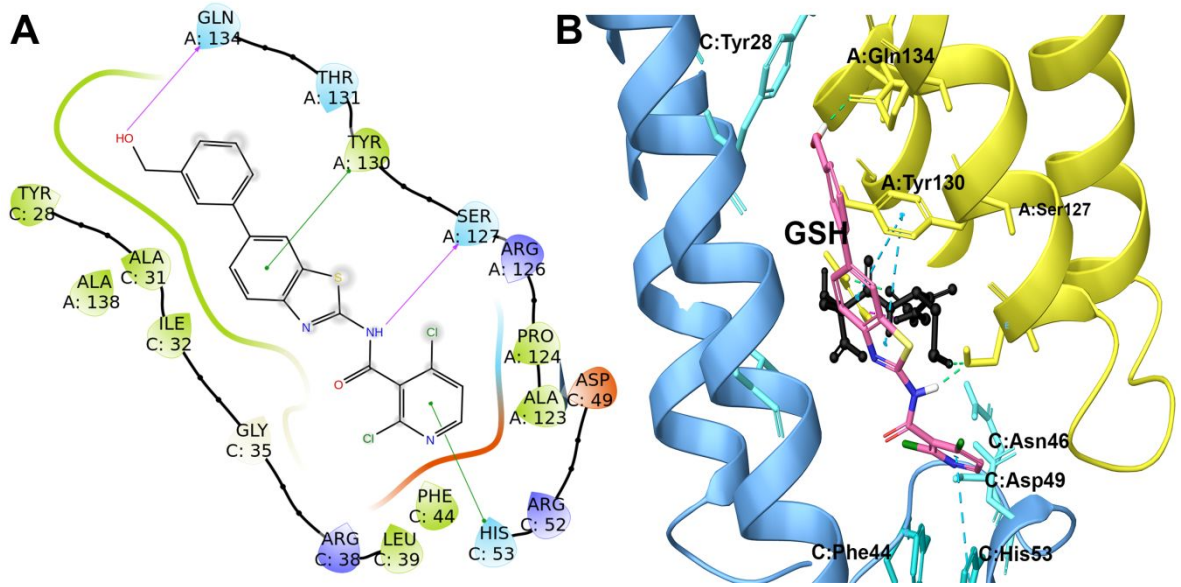

Figure S 6. 2D and 3D representation of the interaction pattern between **4** and mPGES-1.
Panel A) 2D interactions diagram of compound **4** with mPGES-1 receptor counterpart (pdb code: 4BPM); h-bond interactions are reported as purple arrows, while π-π interactions as green lines; GSH is depicted in grey, hydrophobic residues in green, and positive and negative charged residues in blue and red respectively. **Panel B)** 3D representation of compound **4** (pink sticks) in the binding site of mPGES-1 (pdb code: 4BPM). mPGES-1 chain A and its key residues are depicted in yellow ribbons and stick, mPGES-1 chain C and its key residues are in cyan ribbons and stick, GSH is reported as black sticks and balls. All the interactions are represented as dotted lines, green for hydrogen bonds, cyano for π-π interactions, violet for halogen bonds.
The calculated binding mode of **4** provided a predicted energy of binding = -7.6 kcal mol^{-1}.

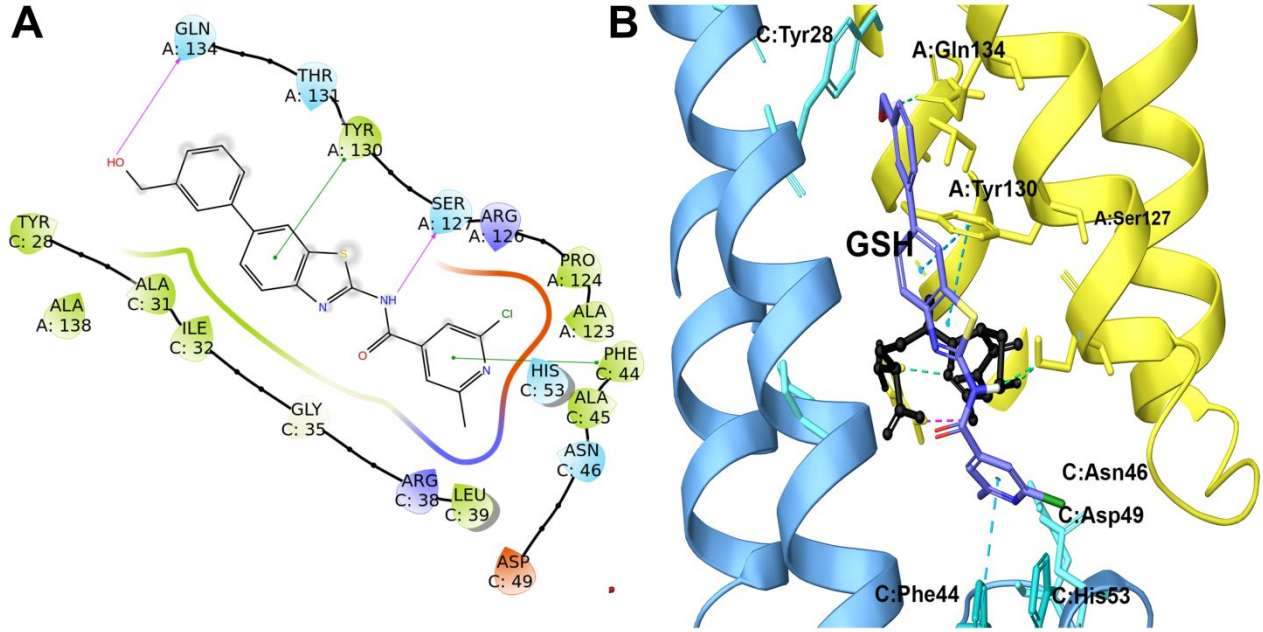

Figure S 7 2D and 3D representation of the interaction pattern between **5** and mPGES-1.
Panel A) 2D interactions diagram of compound **5** with mPGES-1 receptor counterpart (pdb code: 4BPM); h-bond interactions are reported as purple arrows, while π-π interactions as green lines; GSH is depicted in grey, hydrophobic residues in green, and positive and negative charged residues

in blue and red respectively. **Panel B)** 3D representation of compound **5** (light blue sticks) in the binding site of mPGES-1 (pdb code: 4BPM). mPGES-1 chain A and its key residues are depicted in yellow ribbons and stick, mPGES-1 chain C and its key residues are in cyan ribbons and stick, GSH is reported as black sticks and balls. All the interactions are represented as dotted lines, green for hydrogen bonds, cyano for π-π interactions, violet for halogen bonds.
The calculated binding mode of **5** provided a predicted energy of binding = -8.1 kcal mol^{-1}.

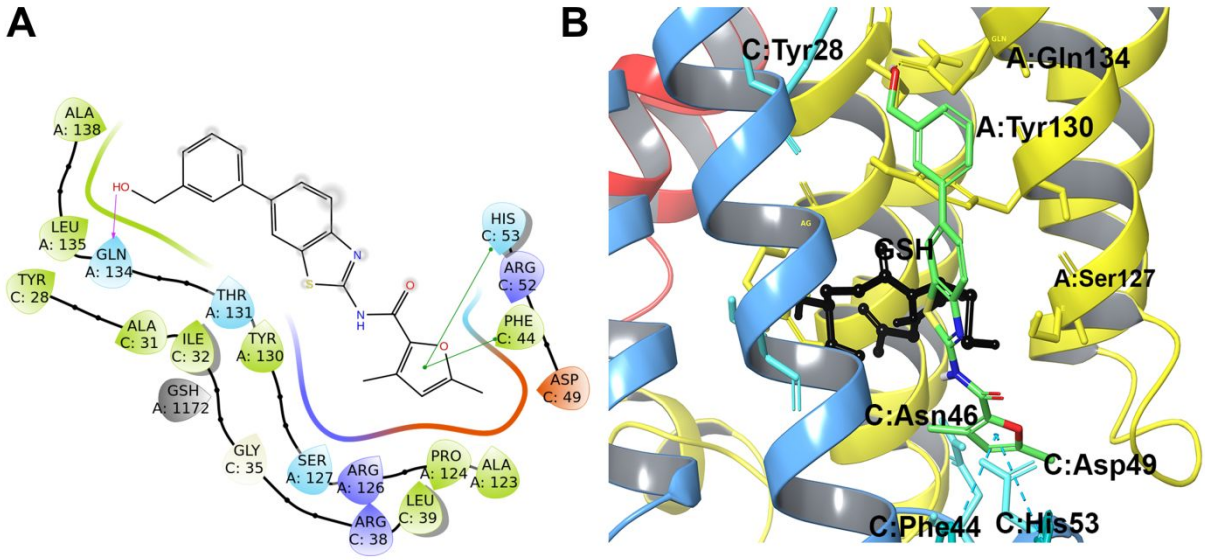

Figure S 8 2D and 3D representation of the interaction pattern between **6** and mPGES-1.
Panel A) 2D interactions diagram of compound **6** with mPGES-1 receptor counterpart (pdb code: 4BPM); h-bond interactions are reported as purple arrows, while π-π interactions as green lines; GSH is depicted in grey, hydrophobic residues in green, and positive and negative charged residues in blue and red respectively. **Panel B)** 3D representation of compound **6** (light green sticks) in the binding site of mPGES-1 (pdb code: 4BPM). mPGES-1 chain A and its key residues are depicted in yellow ribbons and stick, mPGES-1 chain C and its key residues are in cyan ribbons and stick, GSH is reported as black sticks and balls. All the interactions are represented as dotted lines, green for hydrogen bonds, cyano for π-π interactions, violet for halogen bonds.
The calculated binding mode of **5** provided a predicted energy of binding = -7.0 kcal mol^{-1}.

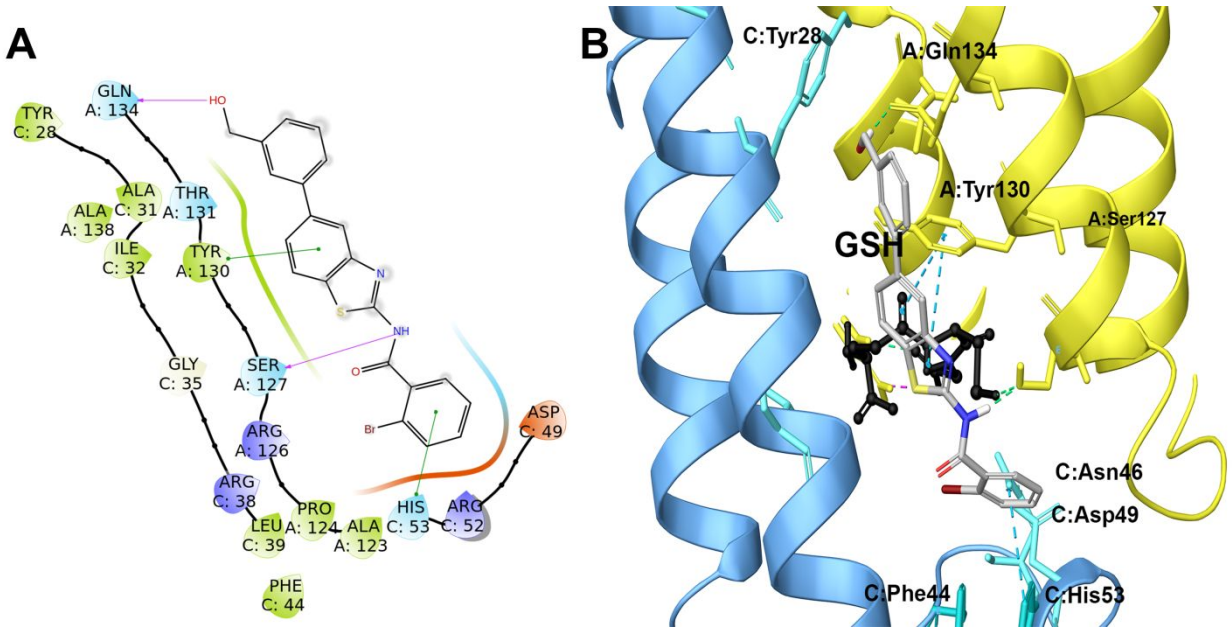

Figure S 9 2D and 3D representation of the interaction pattern between **7** and mPGES-1.
Panel A) 2D interactions diagram of compound **7** with mPGES-1 receptor counterpart (pdb code: 4BPM); h-bond interactions are reported as purple arrows, while π-π interactions as green lines; GSH is depicted in grey, hydrophobic residues in green, and positive and negative charged residues in blue and red respectively. **Panel B)** 3D representation of compound **7** (grey sticks) in the binding site of mPGES-1 (pdb code: 4BPM). mPGES-1 chain A and its key residues are depicted in yellow ribbons and stick, mPGES-1 chain C and its key residues are in cyan ribbons and stick, GSH is reported as black sticks and balls. All the interactions are represented as dotted lines, green for hydrogen bonds, cyano for π-π interactions, violet for halogen bonds.
The calculated binding mode of **7** provided a predicted energy of binding = -7.9 kcal mol^{-1}.

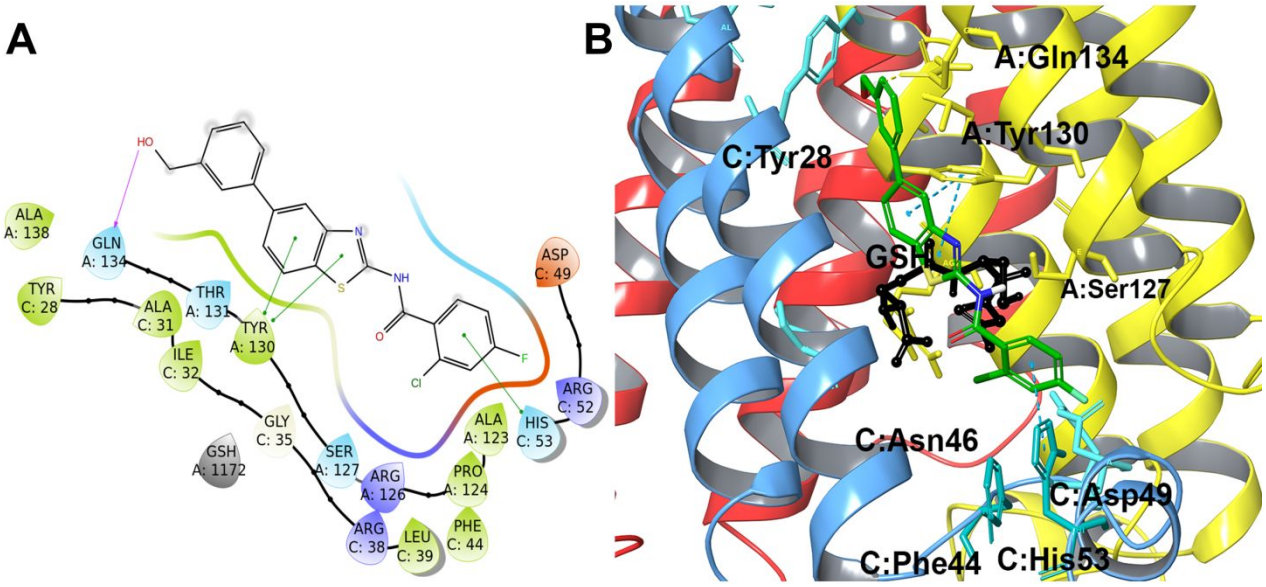

Figure S 10 2D and 3D representation of the interaction pattern between **8** and mPGES-1.
Panel A) 2D interactions diagram of compound **8** with mPGES-1 receptor counterpart (pdb code: 4BPM); h-bond interactions are reported as purple arrows, while π-π interactions as green lines; GSH is depicted in grey, hydrophobic residues in green, and positive and negative charged residues in blue and red respectively. **Panel B)** 3D representation of compound **8** (green sticks) in the binding site of mPGES-1 (pdb code: 4BPM). mPGES-1 chain A and its key residues are depicted in yellow ribbons and stick, mPGES-1 chain C and its key residues are in cyan ribbons and stick, GSH

is reported as black sticks and balls. All the interactions are represented as dotted lines, green for hydrogen bonds, cyano for π-π interactions, violet for halogen bonds.
The calculated binding mode of **8** provided a predicted energy of binding = -7.7 kcal mol^{-1}.

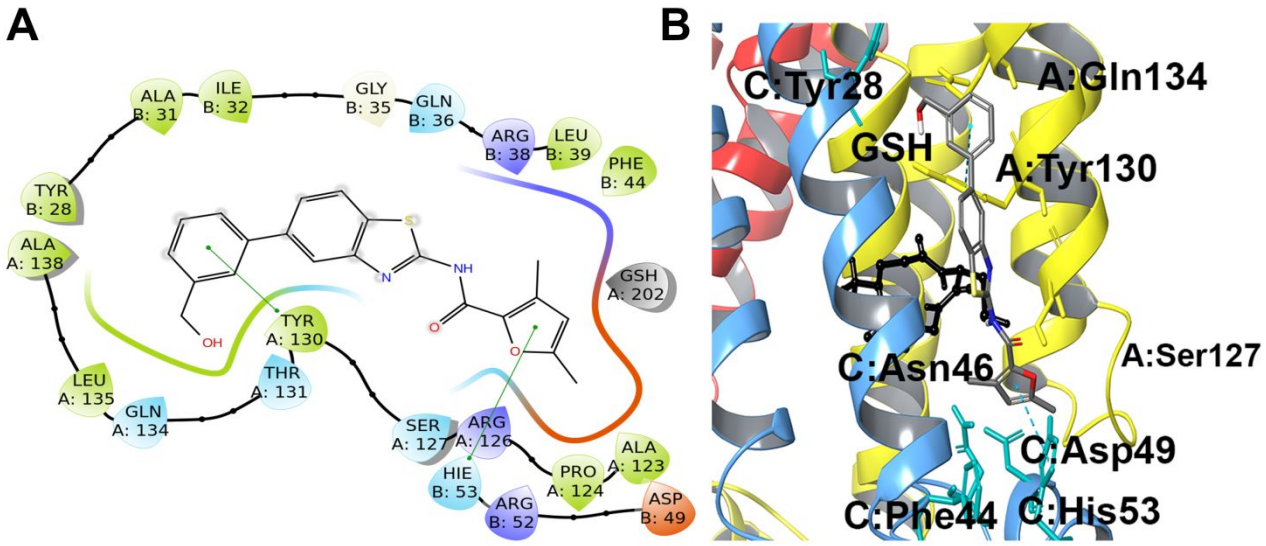

Figure S 11 2D and 3D representation of the interaction pattern between **9** and mPGES-1.
Panel A) 2D interactions diagram of compound **9** with mPGES-1 receptor counterpart (pdb code: 4BPM); h-bond interactions are reported as purple arrows, while π-π interactions as green lines; GSH is depicted in grey, hydrophobic residues in green, and positive and negative charged residues in blue and red respectively. **Panel B)** 3D representation of compound **9** (dark grey sticks) in the binding site of mPGES-1 (pdb code: 4BPM). mPGES-1 chain A and its key residues are depicted in yellow ribbons and stick, mPGES-1 chain C and its key residues are in cyan ribbons and stick, GSH is reported as black sticks and balls. All the interactions are represented as dotted lines, green for hydrogen bonds, cyano for π-π interactions, violet for halogen bonds.
The calculated binding mode of **9** provided a predicted energy of binding = -7.0 kcal mol^{-1}.

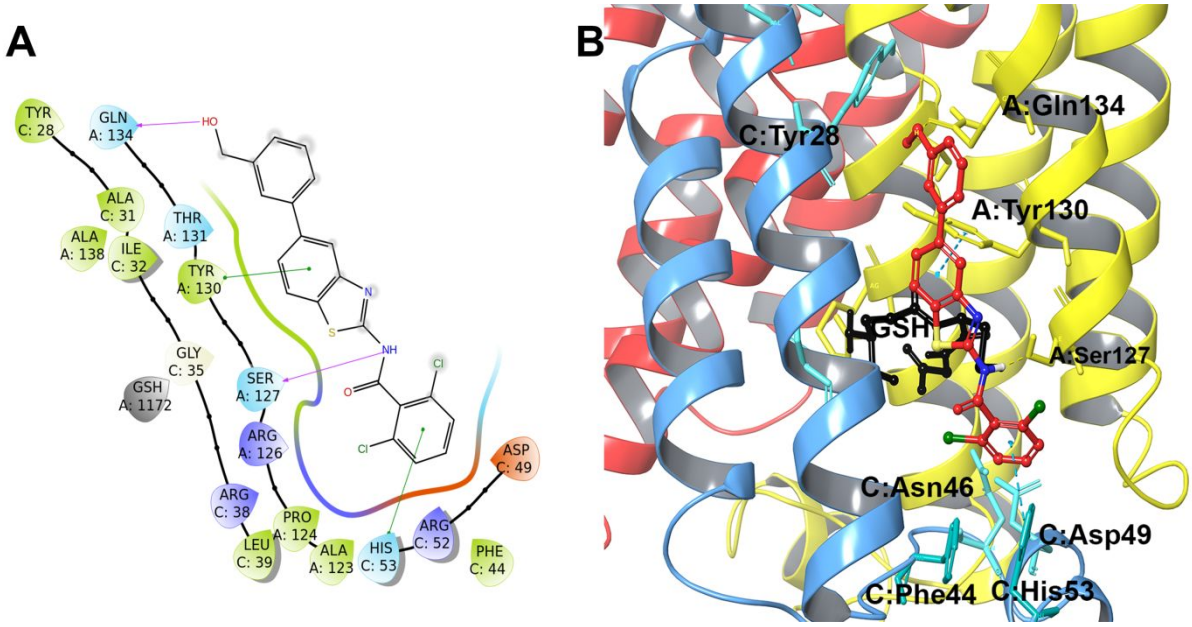

Figure S 12 2D and 3D representation of the interaction pattern between **10** and mPGES-1.
Panel A) 2D interactions diagram of compound **10** with mPGES-1 receptor counterpart (pdb code: 4BPM); h-bond interactions are reported as purple arrows, while π-π interactions as green lines;

GSH is depicted in grey, hydrophobic residues in green, and positive and negative charged residues in blue and red respectively. **Panel B)** 3D representation of compound **10** (red sticks) in the binding site of mPGES-1 (pdb code: 4BPM). mPGES-1 chain A and its key residues are depicted in yellow ribbons and stick, mPGES-1 chain C and its key residues are in cyan ribbons and stick, GSH is reported as black sticks and balls. All the interactions are represented as dotted lines, green for hydrogen bonds, cyano for π-π interactions, violet for halogen bonds.
The calculated binding mode of **10** provided a predicted energy of binding = -7.9 kcal mol^{-1}.

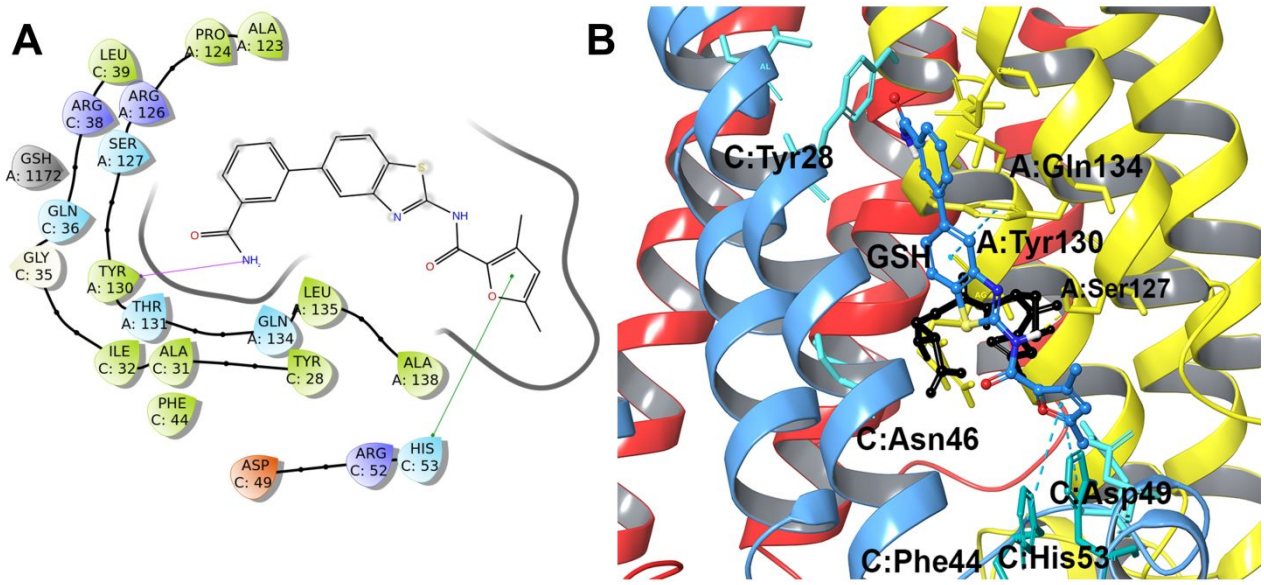

Figure S 13 2D and 3D representation of the interaction pattern between **11** and mPGES-1.
Panel A) 2D interactions diagram of compound **11** with mPGES-1 receptor counterpart (pdb code: 4BPM); h-bond interactions are reported as purple arrows, while π-π interactions as green lines; GSH is depicted in grey, hydrophobic residues in green, and positive and negative charged residues in blue and red respectively. **Panel B)** 3D representation of compound **11** (light blue sticks) in the binding site of mPGES-1 (pdb code: 4BPM). mPGES-1 chain A and its key residues are depicted in yellow ribbons and stick, mPGES-1 chain C and its key residues are in cyan ribbons and stick, GSH is reported as black sticks and balls. All the interactions are represented as dotted lines, green for hydrogen bonds, cyano for π-π interactions, violet for halogen bonds.
The calculated binding mode of **11** provided a predicted energy of binding = -7.0 kcal mol^{-1}

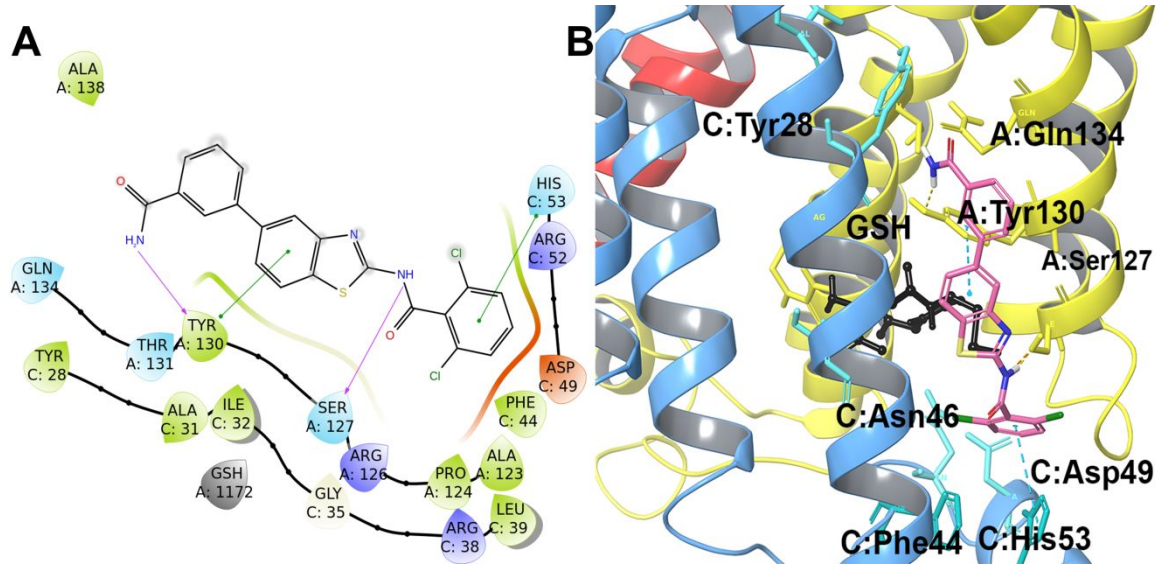

Figure S 14 2D and 3D representation of the interaction pattern between **12** and mPGES-1.
Panel A) 2D interactions diagram of compound **12** with mPGES-1 receptor counterpart (pdb code: 4BPM); h-bond interactions are reported as purple arrows, while π-π interactions as green lines; GSH is depicted in grey, hydrophobic residues in green, and positive and negative charged residues in blue and red respectively. **Panel B)** 3D representation of compound **12** (light pink sticks) in the binding site of mPGES-1 (pdb code: 4BPM). mPGES-1 chain A and its key residues are depicted in yellow ribbons and stick, mPGES-1 chain C and its key residues are in cyan ribbons and stick, GSH is reported as black sticks and balls. All the interactions are represented as dotted lines, green for hydrogen bonds, cyano for π-π interactions, violet for halogen bonds.
The calculated binding mode of **12** provided a predicted energy of binding = -7.6 kcal mol^{-1}.

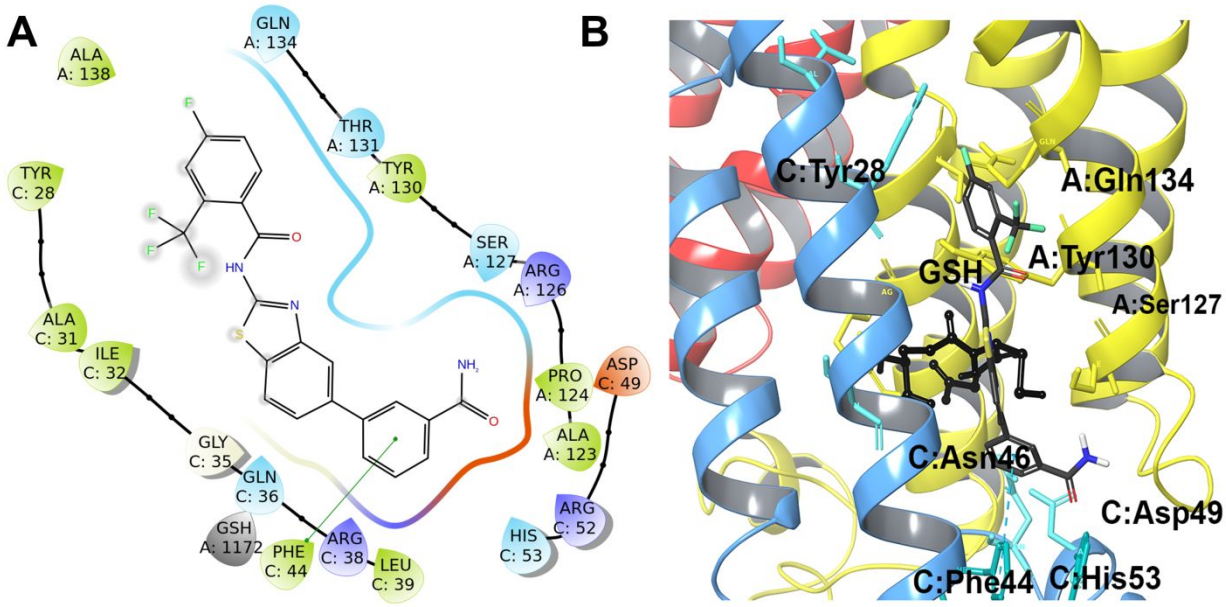

Figure S 15 2D and 3D representation of the interaction pattern between **13** and mPGES-1.
Panel A) 2D interactions diagram of compound **13** with mPGES-1 receptor counterpart (pdb code: 4BPM); h-bond interactions are reported as purple arrows, while π-π interactions as green lines; GSH is depicted in grey, hydrophobic residues in green, and positive and negative charged residues in blue and red respectively. **Panel B)** 3D representation of compound **13** (black sticks) in the binding site of mPGES-1 (pdb code: 4BPM). mPGES-1 chain A and its key residues are depicted in yellow ribbons and stick, mPGES-1 chain C and its key residues are in cyan ribbons and stick, GSH is reported as black sticks and balls. All the interactions are represented as dotted lines, green for hydrogen bonds, cyano for π-π interactions, violet for halogen bonds.
The calculated binding mode of **13** provided a predicted energy of binding = -7.3 kcal mol^{-1}.

Pan-Assay Interference compounds (PAINS) screening

Before the synthetic phase, SwissADME web tool[13] evaluates the presence of chemical moieties belonging to "Pan-Assay Interference Compounds" (PAINS) chemical class.

Since the promiscuity of 2-aminothiazoles is well-known, selected **1-13** compounds were analyzed with SwissADME in order to apply a further filter focused on PAINS identification. All the

molecules belonging to the small library selected for the synthesis (**1**-**13**) passed the filter, as they do not contain PAINS.

General synthetic methods

All commercially available starting materials were purchased from Sigma-Aldrich and were used without any purification. All solvents used for the synthesis were of HPLC grade; they were purchased from Sigma-Aldrich and Carlo Erba Reagenti. ^{1}H NMR spectra were recorded on 300 or 400 MHz Bruker Avance instrument. All compounds were dissolved in 0.5 mL of the following solvents: chloroform-d (Sigma-Aldrich, 99.8 Atom % D); methanol-d_4 (Sigma-Aldrich, 99.8 Atom % D); dimethylsulfoxyde-d_6 (Sigma-Aldrich, 99.8 Atom % D). Coupling constants (*J*) are reported in Herz, and chemical shifts are expressed in parts per million (ppm) on the delta (δ) scale relative to $CHCl_3$ (7.19 ppm for ^{1}H and 77.0 ppm for ^{13}C) or CH_3OH (3.31 ppm for ^{1}H and 49.15 ppm for ^{13}C) or DMSO (2.50 ppm for ^{1}H and 39.51 ppm for ^{13}C) as internal reference. Multiplicities are reported as follows: s, singlet; d, doublet; t, triplet; m, multiplet; dd, doublet of doublets. The solvent signal and the residual HDO signal were labelled with an asterisk. ^{13}C NMR spectra were obtained at 100 MHz and referenced to the internal solvent signal. DEPTQ experiments (dept polarization transfer with decoupling during acquisition using shaped pulse for 180 degree pulse on f1channel) were acquired at 100 MHz. The solvent signal in the spectra was labelled with an asterisk. High-Resolution Mass Spectrometry spectra (HRMS) were acquired on a Bruker SolariX XR 7T (Bruker Daltonics, Bremen Germany). Samples were infused at 2 microliters/min in ESI positive or negative ionization, in a time domain of 2 megawards accumulating 32 spectra. Interface temperature 200°C, nebulizing and drying gas 1.5 and 4L/min. Reactions were monitored on silica gel 60 F254 plates (Merck) and the spots were visualized under UV light. Analytical and semi-preparative reversed-phase HPLC was performed on Agilent Technologies 1200 Series high performance liquid chromatography using a Synergi Fusion C18 reversed-phase column (250 x 4.60mm, 4μ, 80 Å, flow rate = 1 mL/min; 250 x 10.00mm, 10μ, 80 Å, flow rate = 4 mL/min respectively, Phenomenex®). The binary solvent system (A/B) was as follows: 0.1% TFA in water

(A) and 0.1% TFA in CH_3CN (B); gradient condition: from 5% B to 100 % B in 50 min. The absorbance was detected at 280 nm. All tested compounds were obtained with high purity (> 98% detected by HPLC analysis) and were fully characterized by HRMS, and NMR spectra.

Synthesis of 3[3-(2-Amino-benzothiazol-6-yl)-phenyl]-methanol 14

2-Amino-6-bromobenzothiazole (460 mg, 1.0 equiv.), 3-(hydroxymethyl)phenylboronic acid **I** (365 mg, 1.2 equiv.), and tetrakis(triphenylphosphine)palladium(0) (115 mg, 5 mol%), were sequentially added to a degassed mixture of 1,4-dioxane (80%) and water (20%) (10 mL) and the mixture was stirred at r.t. for 30 min. Degassed aqueous Na_2CO_3 solution (1 M, 2 equiv.) was added and the reaction mixture was heated under argon at 80 °C for 16 h. The mixture was transferred to a separating funnel, ethyl acetate was added and the organic layer was washed with brine, separated, and dried over $MgSO_4$. The solvent was removed under reduced pressure, and the residue was purified by chromatography on silica gel eluting with a 1:1 hexane-ethyl acetate mixture to give **14** 0.365 g (75%) as a pale oil.

^{1}H NMR (CD_3OD, 300 MHz):7.74 (d, J = 1.8 Hz, 1H); 7.50 (s, 1H); 7.42 (dd, J = 8.4, 1.9 Hz, 1H); 7.39 (m, 1H); 7.33 (d, J = 8.4 Hz, 1H); 7.28 (t, J = 7.6 Hz, 1H); 7.16 (bd, J = 7.6 Hz, 1H); 4.56 (s, 2H).

Synthesis of [3-(2-Amino-benzothiazol-5-yl)-phenyl]-methanol 15

2-Amino-5-bromobenzothiazole (300 mg, 1.0 equiv.), 3-(hydroxymethyl)phenylboronic acid **I** (237 mg, 1.2 equiv.), and tetrakis(triphenylphosphine)palladium(0) (75 mg, 5 mol%), were sequentially added to a degassed mixture of 1,4-dioxane (80%) and water (20%) (50 mL) and the mixture was stirred at r.t. for 30 min. Degassed aqueous Na_2CO_3 solution (1 M, 2 equiv.) was added and the reaction mixture was heated under argon at 80 °C for 16 h. The mixture was transferred to a separating funnel, ethyl acetate was added and the organic layer was washed with brine, separated, and dried over $MgSO_4$. The solvent was removed under reduced pressure, and the residue was purified by flash chromatography on silica gel eluting with a 3:7 hexane-ethyl acetate mixture to give **15** 0.278 g (88%) as a pale oil.

^{1}H NMR (CD_3OD, 400 MHz): 7.49 (d, *J* = 1.7 Hz, 1H); 7.46 (s, 1H); 7.35 (d, *J* = 8.1 Hz, 1H); 7.30 (dd, *J* = 7.6, 1.7 Hz, 1H); 7.19 (t, *J* = 7.5 Hz, 1H); 7.14 (dd, *J* = 7.6, 1.6 Hz, 1H), 7.10 (dd, *J* = 8.2, 1.8 Hz, 1H); 4.51 (s, 2H).

General procedure for acylation reactions (1-10)

To a solution of **14** or **15** (50 mg, 1 equiv.) in dry acetonitrile (10 mL) and pyridine (0.49 mL, 30 equiv.) chlorotrimethylsilane was added (0.26 mL, 10 equiv.). The resulting mixture was stirred at r.t. for 3 h, then the proper acyl chloride was added (1.5 equiv) and the reaction mixture was stirred overnight. The mixture was diluted with ethyl acetate, washed with 0.5 N HCl (10 mL x 3) and brine (10 mL) and dried ($MgSO_4$). The solvent was removed under reduced pressure, and the residue was purified by semi-preparative reversed-phase HPLC. Yields are reported below for each compound.

2-Chloro-4-fluoro-N-(6-(3-(hydroxymethyl)phenyl)benzo[d]thiazol-2-yl)benzamide (1).

Compound **1** was obtained as a a white solid using **14** and 2-chloro-4-fluorobenzoyl chloride (65% yield).

^{1}H NMR (CD_3OD, 400 MHz): 8.08 (d, *J* = 1.8 Hz, 1H); 7.73 (d, *J* = 8.4 Hz, 1H); 7.64 (dd, *J* = 8.3, 2.1 Hz, 2H); 7.59 (s, 1H); 7.50 (m, 1H); 7.34 (t, *J* = 7.5 Hz, 1H); 7.32 (dd, , *J* = 8.4, 2.5 Hz, 1H); 7.26 (m, 1H) 7.16 (td, *J* = 8.4, 2.5 Hz, 1H); 4.60 (s, 2H).

^{13}C NMR (CD_3OD, 100 MHz): 167.05; 165.28 (d, *J* = 252 Hz);. 160.02; 149.48; 145.29: 143.65; 142.28; 139.06; 134.34 (d, *J* = 13.8 Hz); 132.62 (d, *J* = 9.6 Hz); 132.26 (d, *J* = 3.0 Hz); 130.15; 127.26; 127.12; 126.97; 126.92; 122.30; 120.83; 118.89 (d, *J* = 25.0 Hz); 115.78 (d, *J* = 22.0 Hz); 65.31.

HR-MS: *m/z* calcd for $C_{21}H_{15}ClFN_2O_2S$ $[M+H]^+$ 413.0527; found 413.0523.

2,5-Difluoro-N-(6-(3-(hydroxymethyl)phenyl)benzo[d]thiazol-2-yl)benzamide (2).

Compound **2** was isolated as a a white solid using **14** and 2,5-difluorobenzoyl chloride (72% yield).

^{1}H NMR (CD_3OD, 400 MHz): 8.20 (d, *J* = 1.8 Hz, 1H); 7.87 (d, *J* = 8.4 Hz, 1H); 7.77 (dd, *J* = 8.4, 1.8 Hz, 1H); 7.71 (s, 1H); 7.65 (m, 2H); 7.47 (t, *J* = 7.6 Hz, 1H); 7.40 (m, 3H); 4.72 (s, 2H).

^{13}C NMR (CD_3OD, 100 MHz): 160.1 (d, *J* = 32.0 Hz); 157.6; 156.9 (d, *J* = 214.0 Hz); 156.5 (d, *J* = 228.0 Hz); 147.4; 141.5; 140.9; 137.7; 129.8; 129.1; 126.6; 126.2; 126.2; 125.9; 122.1 (dd, J = 24.5, 9.8 Hz); 121.2; 120.1 (m); 119.8; 118.4 (d, *J* = 26.0 Hz); 118.1 (dd, *J* = 17.0, 8.0 Hz); 65.3.

HR-MS: *m/z* calcd for $C_{21}H_{15}F_2N_2O_2S$ 397.0822 $[M+H]^+$; found 397.0817.

2-Bromo-N-(6-(3-(hydroxymethyl)phenyl)benzo[d]thiazol-2-yl)benzamide (3).

Compound **3** was isolated as a a colorless oil using **14** and 2-bromobenzoyl chloride (78% yield).

^{1}H NMR (CD_3OD, 400 MHz): 8.19 (d, *J* = 1.8 Hz, 1H); 7.85 (d, *J* = 8.4 Hz, 1H); 7.76 (d, *J* = 8.2 Hz, 2H); 7.71 (s, 1H); 7.62 (m, 2H); 7.54 (td, *J* = 7.5, 1.2 Hz, 1H); 7.47 (m, 2H); 7.37 (d, *J* = 7.5 Hz, 1H); 4.72 (s, 2H).

^{13}C NMR (CD_3OD, 100 MHz): 168.7; 160.0; 149.5; 143.6; 142.2; 139.0; 138.0; 134.6; 134.4; 133.7; 133.3; 130.4; 130.1; 128.9; 127.2; 127.1; 126.95; 126.92; 122.3; 120.8; 65.3.

HR-MS: *m/z* calcd for $C_{21}H_{14}BrN_2O_2S$ $[M-H]^-$437.0038; found 436.9964.

2,4-Dichloro-N-(6-(3-(hydroxymethyl)phenyl)benzo[d]thiazol-2-yl)nicotinamide (4).

Compound **4** was isolated as a white solid using **14** and 2,4-dichloropyridine-3-carbonyl chloride (51% yield).

^{1}H NMR (CD_3OD, 400 MHz): 8.48 (d, *J* = 5.5 Hz, 1H); 8.22 (d, *J* = 1.8 Hz, 1H); 7.87 (d, *J* = 8.5 Hz, 1H); 7.77 (dd, *J* = 8.5, 1.8 Hz, 1H); 7.71 (s, 1H); 7.66 (d, *J* = 5.4 Hz, 1H); 7.62 (d, *J* = 8.0 Hz, 1H); 7.45 (t, *J* = 7.6 Hz, 1H); 7.37 (d, *J* = 7.7 Hz, 1H); 4.71 (s, 2H).

HR-MS: *m/z* calcd for $C_{20}H_{14}Cl_2N_3O_2S$ $[M+H]^+$ 430.0184; found 430.0192.

2-Chloro-N-(6-(3-(hydroxymethyl)phenyl)benzo[d]thiazol-2-yl)-6-methylisonicotinamide (5).

Compound **5** was isolated as a a white solid using **14** and 2-chloro-6-methylpyridine-4-carbonyl chloride (53% yield).

^{1}H NMR ($CDCl_3$, 400 MHz): 8.03 (d, J = 1.6 Hz, 1H); 7.87 (m, 3H); 7.80 (dd, *J* = 8.5, 1.7 Hz, 1H); 7.59 (s, 1H); 7.51 (d, *J* = 7.5 Hz, 1H); 7.44 (t, *J* = 7.6 Hz, 1H); 7.35 (d, *J* = 7.5 Hz, 1H); 4.77 (s, 2H); 2.63 (s, 3H).

HR-MS: *m/z* calcd for $C_{21}H_{17}ClN_3O_2S$ $[M+H]^+$ 410.0730; found 410.0738.

N-(6-(3-(hydroxymethyl)phenyl)benzo[d]thiazol-2-yl)-3,5-dimethylfuran-2-carboxamide (6).

Compound **6** was isolated as a a colorless oil using **14** and 2,5-dimethylfuran-3-carbonyl chloride (80% yield).

^{1}H NMR ($CDCl_3$, 400 MHz): 7.96 (d, *J* = 1.6 Hz, 1H); 7.83 (d, *J* = 8.5 Hz, 1H); 7.75 (d, *J* = 8.5 Hz, 1H); 7.58 (s, 1H); 7.49 (d, *J* = 7.8 Hz, 1H); 7.42 (t, *J* = 7.6 Hz, 1H); 7.34 (d, *J* = 7.5 Hz, 1H); 6.77 (s, 1H); 4.75 (s, 2H); 2.61 (s, 3H); 2.27 (s, 3H).

^{13}C NMR ($CDCl_3$, 100 MHz): 162.0; 161.7; 160.4; 151.2; 141.7; 140.3; 138.6; 129.9; 129.2; 127.1; 126.6; 126.3; 125.8; 120.0; 118.3; 114.5; 113.9; 103.7; 65.1; 14.1; 13.3.

HR-MS: *m/z* calcd for $C_{21}H_{19}N_2O_3S$ $[M+H]^+$ 379.1116; found 379.1112.

2-Bromo-N-(5-(3-(hydroxymethyl)phenyl)benzo[d]thiazol-2-yl)benzamide (7).

Compound **7** was isolated as a a colorless oil using **15** and 2-bromobenzoyl chloride (78% yield).

^{1}H NMR ($CDCl_3$, 400 MHz): 7.89 (m, 2H); 7.77 (dd, *J* = 7.6, 1.8 Hz, 1H); 7.61 (m, 3H); 7.53 (m, 1H); 7.44 (t, *J* = 7.6 Hz, 1H); 7.39 (m, 2H); 7.31 (td, *J* = 7.7, 1.8 Hz, 1H); 4.77 (s, 2H).

^{13}C NMR ($CDCl_3$, 100 MHz): 165.7; 161.0; 144.9; 141.5; 140.6; 140.4; 134.1; 133.9; 132.9; 130.1; 129.1; 129.0; 127.7; 126.7; 126.3; 125.9; 124.3; 121.8; 120.2; 117.5; 65.2.

HR-MS: *m/z* calcd for $C_{21}H_{16}BrN_2O_2S$ $[M+H]^+$ 439.0116; found 439.0107.

2-Chloro-4-fluoro-N-(5-(3-(hydroxymethyl)phenyl)benzo[d]thiazol-2-yl)benzamide (8).

Compound **8** was obtained as a a white solid using **15** and 2-chloro-4-fluorobenzoyl chloride (82% yield).

^{1}H NMR ($CDCl_3$, 400 MHz): 7.85 (d, *J* = 8.3 Hz, 1H); 7.77 (dd, *J* = 8.7, 5.9 Hz, 1H); 7.58 (m, 2H); 7.44 (m, 3H); 7.38 (m, 1H); 6.90 (dd, *J* = 8.3, 2.4 Hz, 1H); 6.84 (td, *J* = 8.1, 2.4 Hz, 1H); 4.77 (s, 2H).

^{13}C NMR ($CDCl_3$, 100 MHz): 164.5 (d, *J* = 255 Hz); 163.47; 161.45; 158.25; 141.78; 141.33; 140.02; 134.37; 132.8 (d, *J* = 9.8 Hz); 129.59; 129.29; 127.21; 126.62; 126.60; 125.99; 125.00; 122.25; 118.88 (d, *J* = 25.0 Hz); 116.99; 115.20 (d, *J* = 21.8 Hz); 65.18.

HR-MS: *m/z* calcd for $C_{21}H_{15}ClFN_2O_2S$ $[M+H]^+$ 413.0527; found 413.0519.

N-(5-(3-(hydroxymethyl)phenyl)benzo[d]thiazol-2-yl)-3,5-dimethylfuran-2-carboxamide (9).

Compound **9** was isolated as a a colorless oil using **15** and 2,5-dimethylfuran-3-carbonyl chloride (65% yield).

^{1}H NMR ($CDCl_3$, 400 MHz): 7.83 (d, *J* = 8.2 Hz, 1H); 7.77 (d, *J* = 1.5 Hz, 1H); 7.56 (s, 1H); 7.51 (dd, *J* = 8.2, 1.5 Hz, 1H); 7.48 (m, 1H); 7.42 (t, *J* = 7.5 Hz, 1H); 7.35 (m, 1H); 6.28 (s, 1H); 4.76 (s, 2H); 2.63 (s, 3H); 2.17 (s, 3H).

^{13}C NMR ($CDCl_3$, 100 MHz): 162.74; 161.44; 160.72; 151.49; 141.85; 141.68; 139.77; 129.31; 129.10; 126.69; 126.52; 125.81; 125.04; 122.35; 115.75; 113.73; 113.67; 103.98; 65.09; 14.05; 13.24.

HR-MS: *m/z* calcd for $C_{21}H_{19}N_2O_3S$ $[M+H]^+$ 379.1116; found 379.1111.

2,6-Dichloro-N-(5-(3-(hydroxymethyl)phenyl)benzo[d]thiazol-2-yl)benzamide (10).

Compound **10** was obtained as a a white solid using **15** and 2,6-dichlorobenzoyl chloride (85% yield).

^{1}H NMR ($CDCl_3$, 400 MHz): 7.83 (d, *J* = 8.3 Hz, 1H); 7.59 (s, 1H); 7.53 (dd, *J* = 8.4, 1.4 Hz, 1H); 7.49 (m, 2H); 7.39 (m, 1H); 7.36 (s, 1H); 6.84 (m, 2H); 6.77 (dd, *J* = 9.3, 6.6 Hz, 1H); 4.81 (s, 2H).
^{13}C NMR (DMSO-d_6 100 MHz): 163.2; 157.9; 149.3; 143.3; 139.7; 139.0; 134.2; 132.3; 131.1; 130.6; 128.8; 128.3; 125.6; 125.3; 125.0; 123.0; 122.3; 118.0; 62.9.
HR-MS: *m/z* calcd for $C_{21}H_{15}Cl_2N_2O_2S$ $[M+H]^+$ 429.0231; found 429.0224.

General procedure for the preparation of compounds 16-18

To a solution of 2-amino-5-bromobenzothiazole (200 mg, 1 equiv.) in dry acetonitrile (20 mL) and pyridine (0.11 mL, 1.5 equiv.) the proper acyl chloride was added (1.2 equiv) and the reaction mixture was stirred overnight. The mixture was diluted with ethyl acetate, washed with water (10 mL x 2) and brine (10 mL) and dried ($MgSO_4$). The solvent was removed under reduced pressure, and the residue was purified by flash chromatography on silica gel eluting with a 3:7 hexane-ethyl acetate mixture.

N-(5-bromobenzo[d]thiazol-2-yl)-3,5-dimethylfuran-2-carboxamide (16).

Compound **16** was isolated as a colourless oil using 2,5-dimethylfuran-3-carbonyl chloride (83 % yield).
^{1}H NMR ($CDCl_3$/CD_3OD 1:1, 300 MHz): 7.86 (d, *J* = 1.9 Hz, 1H); 7.69 (d, *J* = 8.4 Hz, 1H); 7.37 (dd, *J* = 8.5, 1.9 Hz, 1H); 6.49 (s, 1H); 2.58 (s, 3H); 2.27 (s, 3H).

N-(5-bromobenzo[d]thiazol-2-yl)-2,6-dichlorobenzamide (17).

Compound **17** was isolated as a colorless oil using 2,6-dichlorobenzoyl chloride (75% yield).
^{1}H NMR ($CDCl_3$, 400 MHz): 8.69 (d, *J* = 1.7 Hz, 1H); 7.53 (dd, *J* = 8.3, 1.8 Hz, 1H); 7.46 (d, *J* = 8.3 Hz, 1H); 6.83 (m, 2H); 6.83 (dd, *J* = 8.8, 7.3 Hz, 1H).

N-(5-bromobenzo[d]thiazol-2-yl)-4-fluoro-2-(trifluoromethyl)benzamide (18).

Compound **18** was isolated as a colorless oil using 4-fluoro-2-(trifluoromethyl)benzoyl chloride (93% yield).
^{1}H NMR (DMSO-d_6, 400 MHz): 8.28 (d, *J* = 1.8 Hz, 1H); 8.08 (dd, *J* = 8.7, 5.2 Hz, 1H); 7.99 (d, *J* = 8.2 Hz, 1H); 7.88 (dd, *J* = 9.2, 2.5 Hz, 1H); 7.74 (dd, *J* = 8.2, 1.8 Hz, 1H); 7.68 (m, 1H).

General procedure for the preparation of compounds 11-13

Compound **16, 17** or **18** (1.0 equiv.), 3-aminocarbonylphenylboronic acid **II** (1.2 equiv.), and tetrakis(triphenylphosphine)palladium(0) (5 mol%), were sequentially added to a degassed mixture of 1,4-dioxane (80%) and water (20%) (50 mL) and the mixture was stirred at r.t. for 30 min. Degassed aqueous Na_2CO_3 solution (1 M, 2 equiv.) was added and the reaction mixture was heated under argon at 80 °C for 16 h. The mixture was transferred to a separating funnel, ethyl acetate was added and the organic layer was washed with brine, separated, and dried over $MgSO_4$. The solvent was removed under reduced pressure, and the residue was purified purified by semi-preparative reversed-phase HPLC.

N-(5-(3-carbamoylphenyl)benzo[d]thiazol-2-yl)-3,5-dimethylfuran-2-carboxamide (11).

Compound **11** was obtained from **16** and isolated as a white solid (32% yield).

^{1}H NMR ($CDCl_3$, 400 MHz): 8.08 (s, 1H); 8.00 (s, 1H); 7.91 (d, *J* = 8.3 Hz, 1H); 7.84 (d, *J* = 7.7 Hz, 2H); 7.70 (d, *J* = 8.5 Hz, 1H); 7.59 (t, *J* = 7.9 Hz, 1H); 6.81 (s, 1H); 2.65 (s, 3H); 2.31 (s, 3H).

^{13}C NMR (DMSO-d_6, 100MHz): 167.9; 162.1; 159.1; 158.0; 157.7;149.8; 149.4; 140.2; 138.1; 135.0; 129.8; 129.0; 126.6; 125.9; 122.7; 122.2; 118.4; 115.8; 104.8; 13.7; 13.1.

HR-MS: *m/z* calcd for $C_{21}H_{18}N_3O_3S$ $[M+H]^+$ 392.1069; found 392.1068.

N-(5-(3-carbamoylphenyl)benzo[d]thiazol-2-yl)-2,6-dichlorobenzamide (12).

Compound **12** was obtained from **17** and isolated as a white solid (42% yield).

^{1}H NMR ($CDCl_3$, 400 MHz): 8.52 (d, *J* = 8.4 Hz, 1H); 7.65 (d, *J* = 7.6 Hz, 1H); 7.53 (dd, *J* = 8.5, 7.5 Hz, 1H); 7.44 (m, 1H); 7.14 (m, 3H); 6.98 (d, *J* = 8.4 Hz, 2H); 6.87 (dd, *J* = 8.8, 7.3 Hz, 1H).

^{13}C NMR ($CDCl_3$, 100MHz): 173.98; 167.69; 164.42; 138.01; 137.18; 136.27; 133.51; 131.39; 131.05; 129.80; 129.44; 128.56; 128.20; 127.26; 127.13; 126.55; 125:49; 122.58; 117.52.

HR-MS: *m/z* calcd for $C_{21}H_{14}Cl_2N_3O_2S$ $[M+H]^+$ 442.0184; found 442.2975 .

N-(5-(3-carbamoylphenyl)benzo[d]thiazol-2-yl)-4-fluoro-2-(trifluoromethyl)benzamide (13).

Compound **13** was obtained from **18** and isolated as a white solid (45% yield).

^{1}H NMR (DMSO-d_6 400 MHz): 8.27 (s, 1H); 8.14 (m, 3H); 7.95 (dd, *J* = 8.6, 5.4 Hz, 1H); 7.86 (m, 2H); 7.72 (m, 3H).

^{13}C NMR (DMSO-d_6 100 MHz):165.7; 162.5 (d, *J* = 250.0 Hz); 158.7; 157.8 (d, *J* = 30.7 Hz); 149.2; 141.1; 136.5; 132.0 (d, *J* = 8.8 Hz); 131.8; 131.7; 131.1; 130.5; 130.2; 129.9; 128.7 (dd, *J* = 32.6, 8.5 Hz); 122.9; 122.6 (q, *J* = 270.0 Hz); 122.5; 119.6 (d, *J* = 21.4 Hz); 118.9; 118.8; 114.5

(dd, J = 26.0, 4.7 Hz).

HR-MS: *m/z* calcd for $C_{22}H_{14}F_4N_3O_2S$ $[M+H]^+$ 460.0743; found = 459.8991.

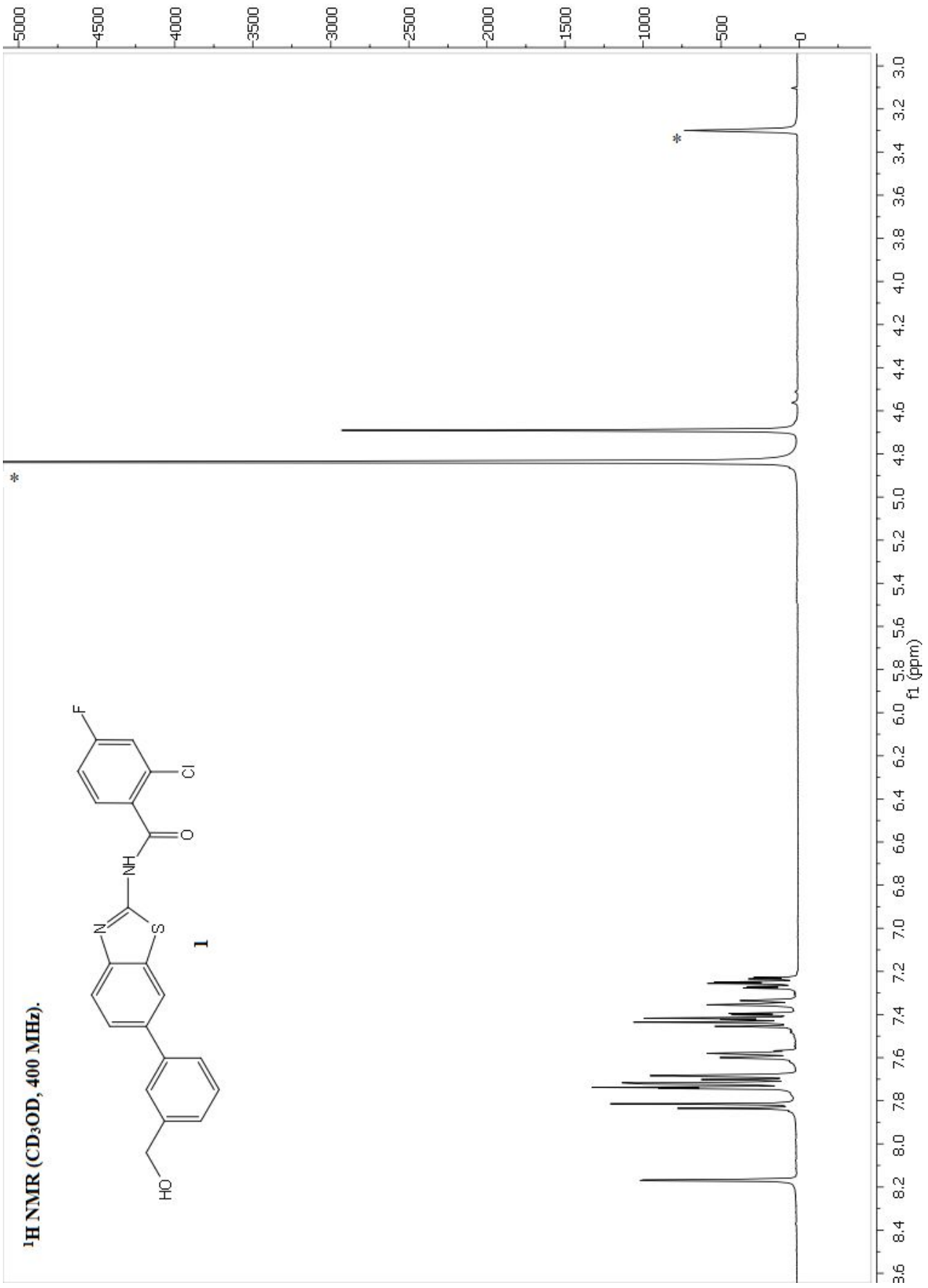

Figure S 16. Compound **1** ^{1}H NMR (CD_3OD, 400 MHz).

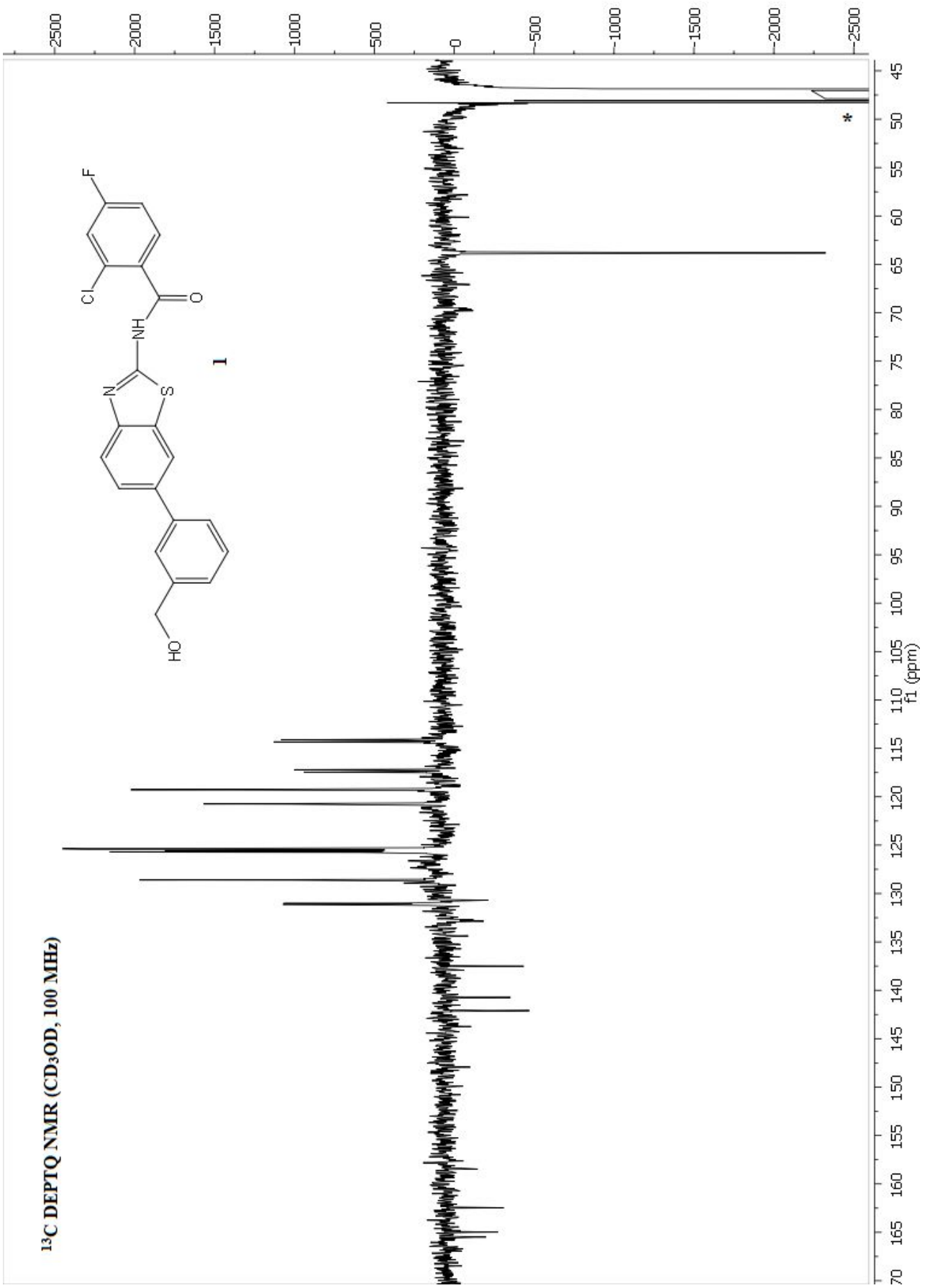

Figure S 17. Compound **1** ^{13}C DEPTQ NMR (CD_3OD, 100 MHz).

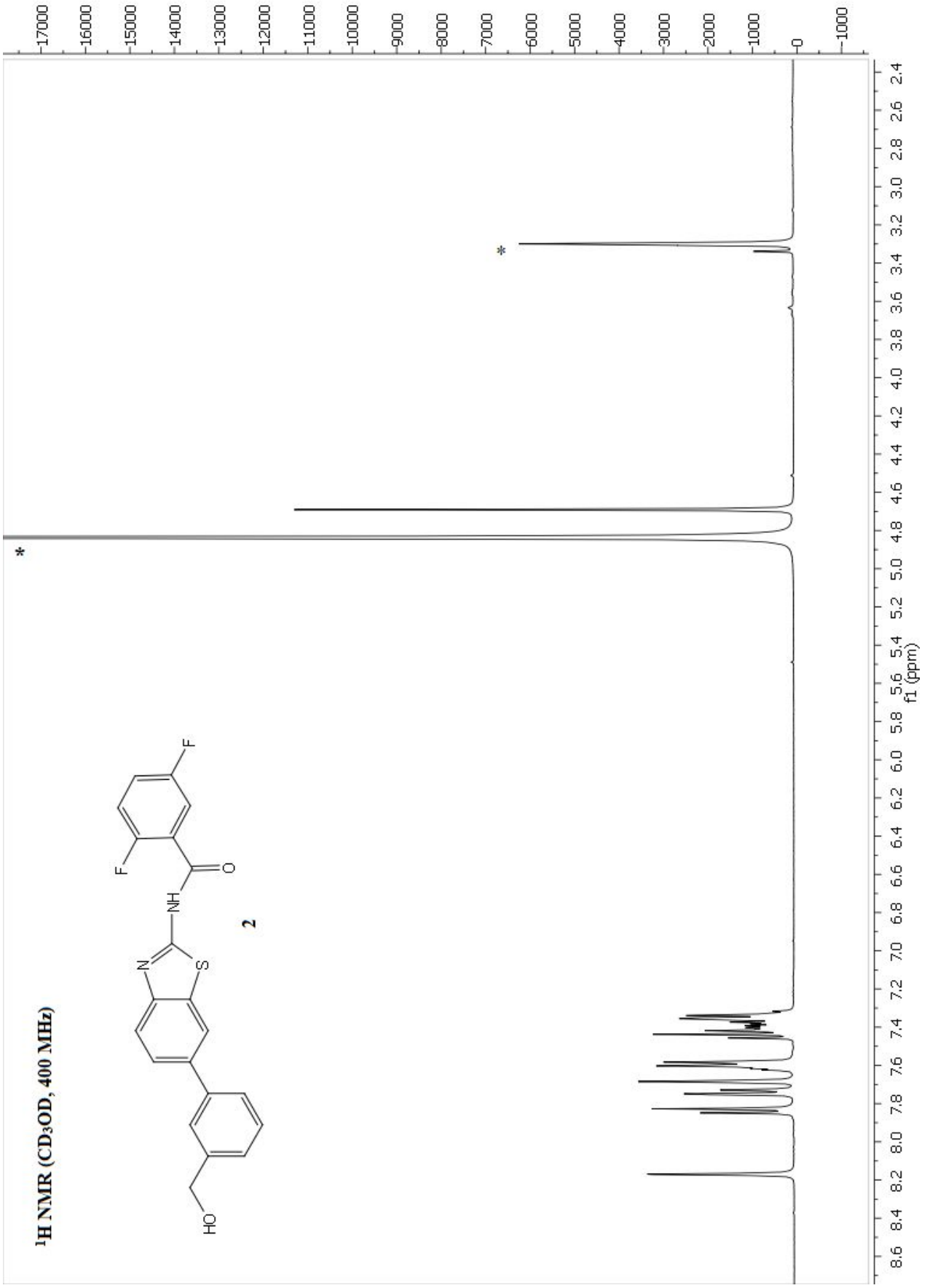

Figure S 18. Compound **2** ^{1}H NMR (CD_3OD, 400 MHz).

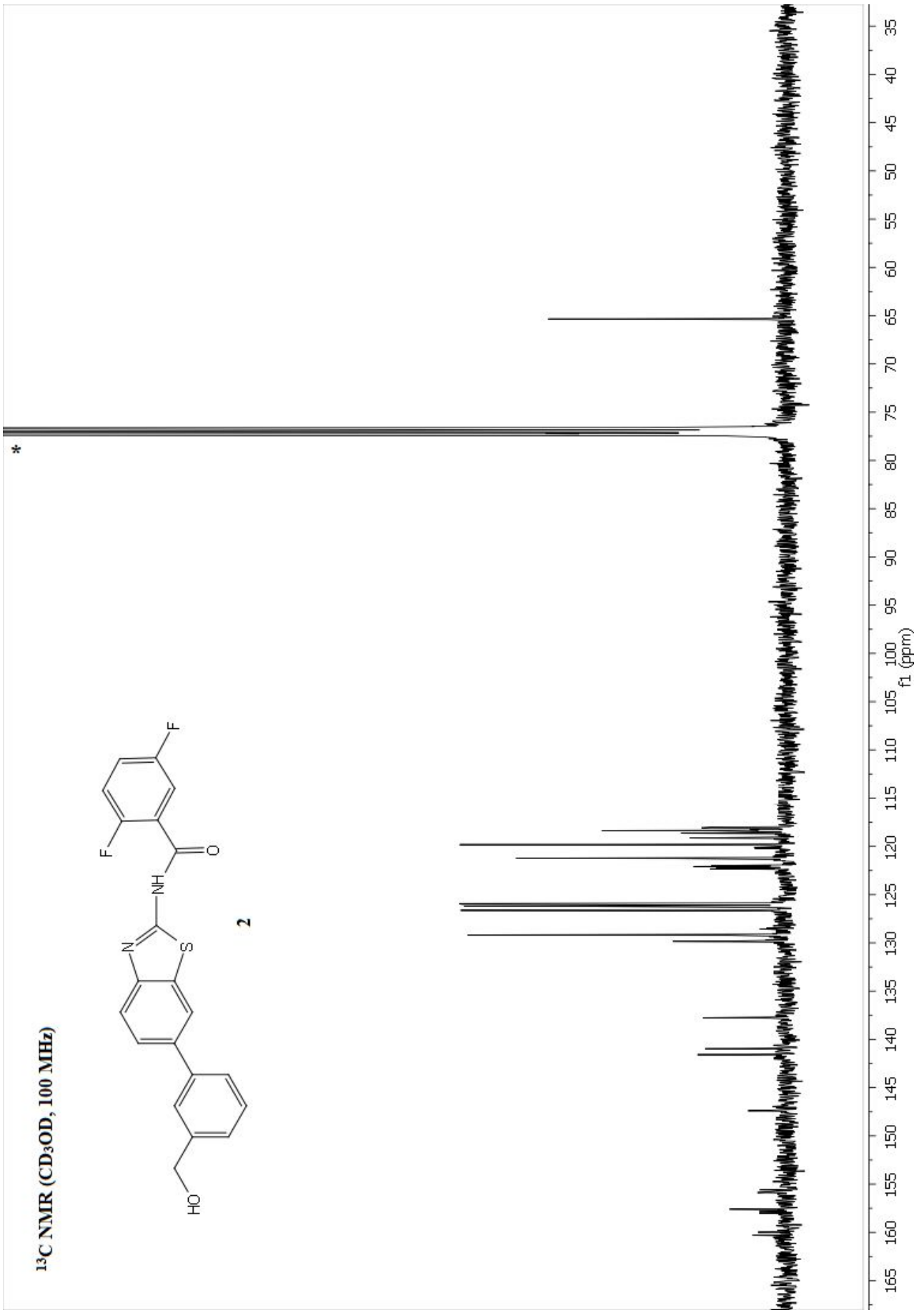

Figure S 19 Compound **2** ^{13}C NMR (CD_3OD, 100 MHz).

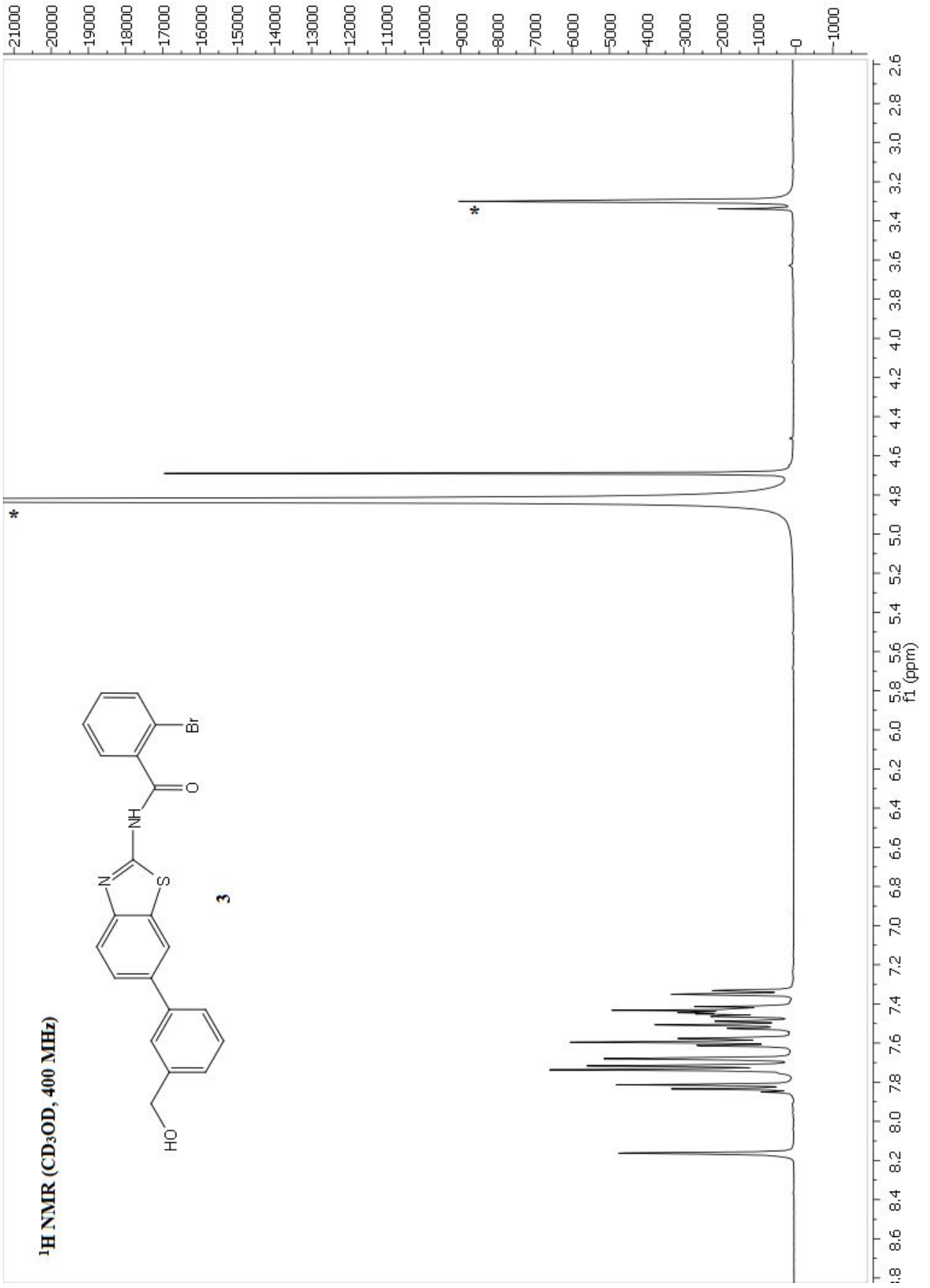

Figure S 20 Compound **3** ^{1}H NMR (CD_3OD, 400 MHz).

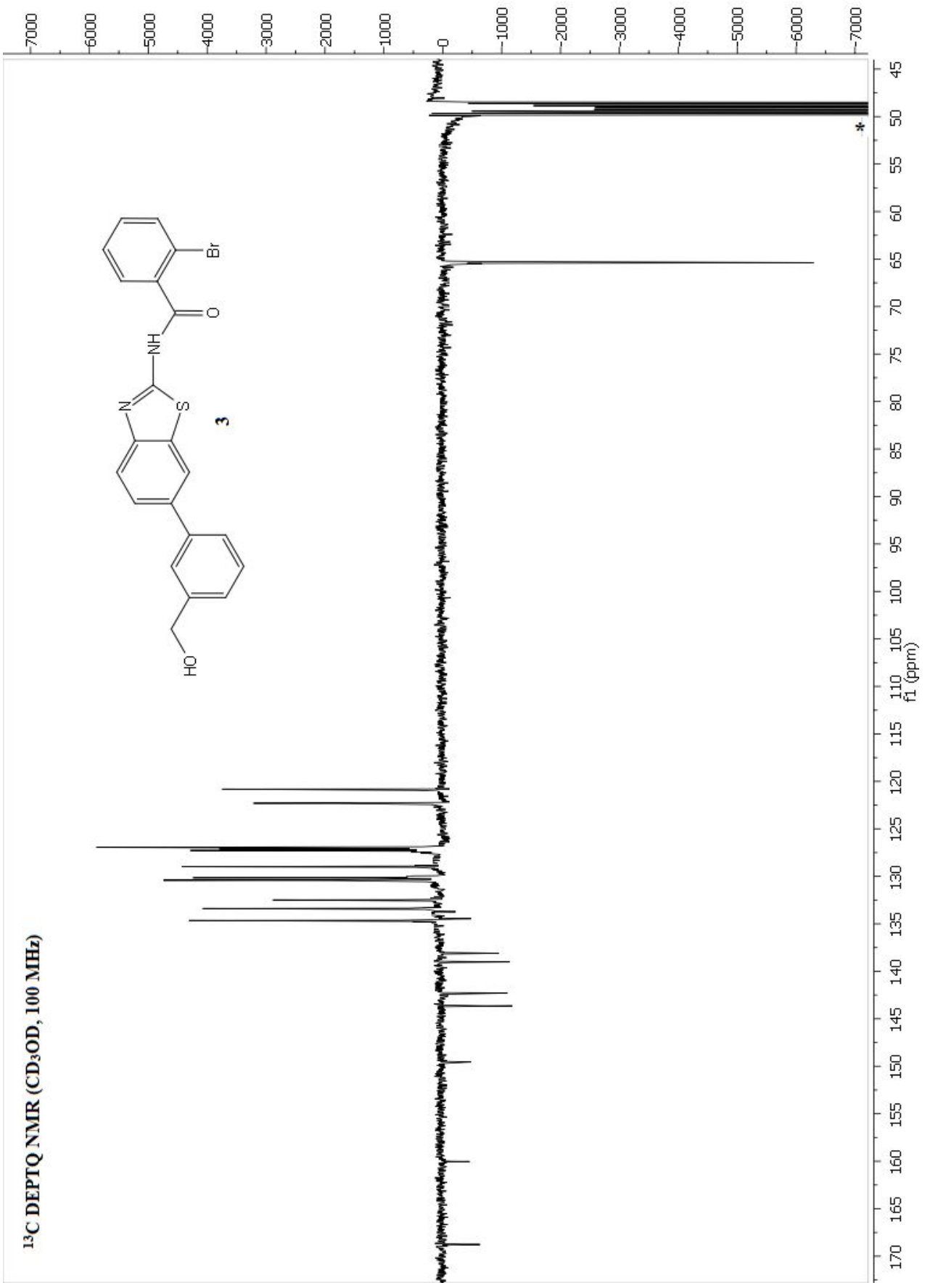

Figure S 21. Compound **3** ^{13}C DEPTQ NMR (CD_3OD, 100 MHz).

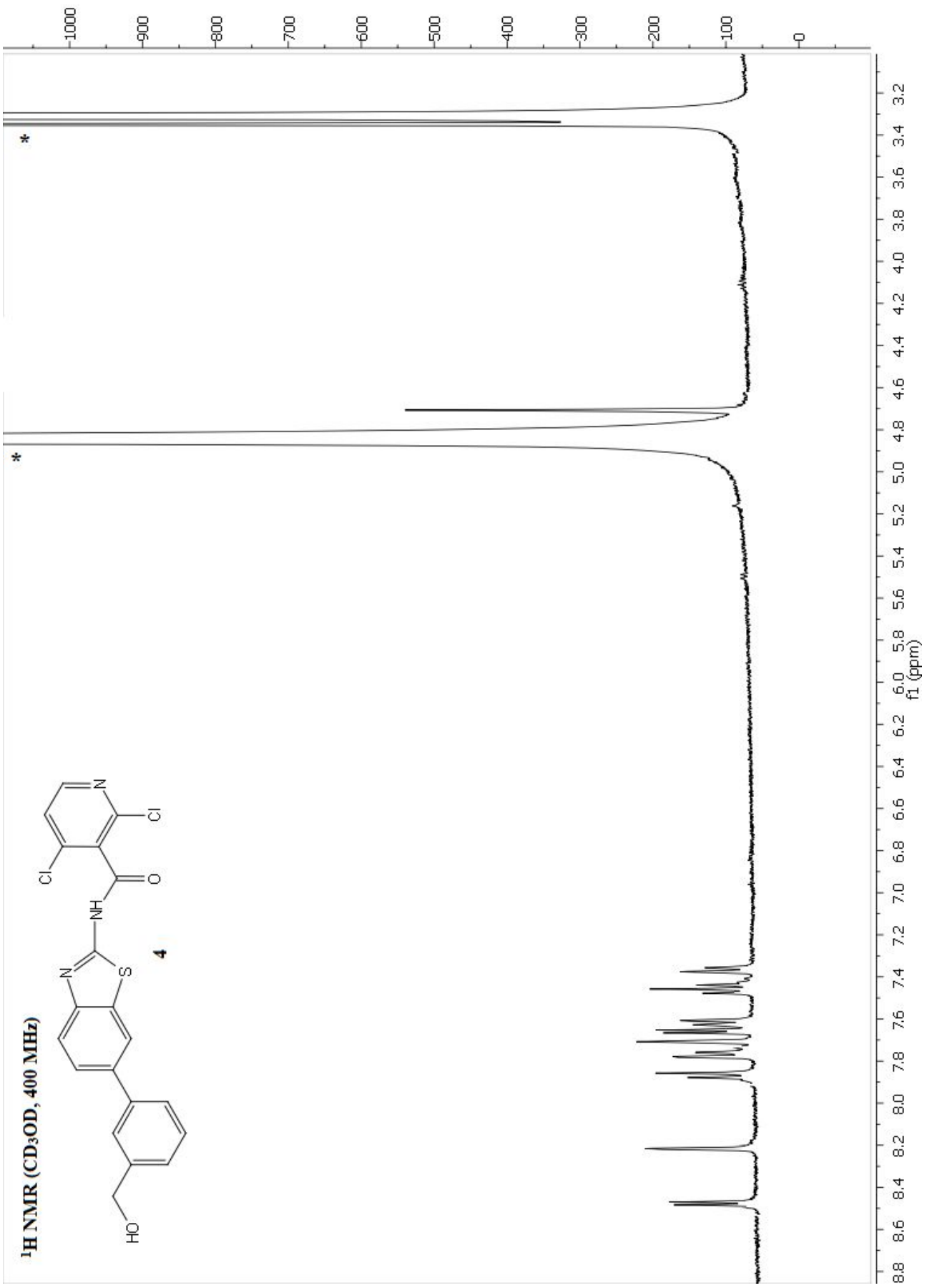

Figure S 22. Compound **4** ^{1}H NMR (CD_3OD, 400 MHz).

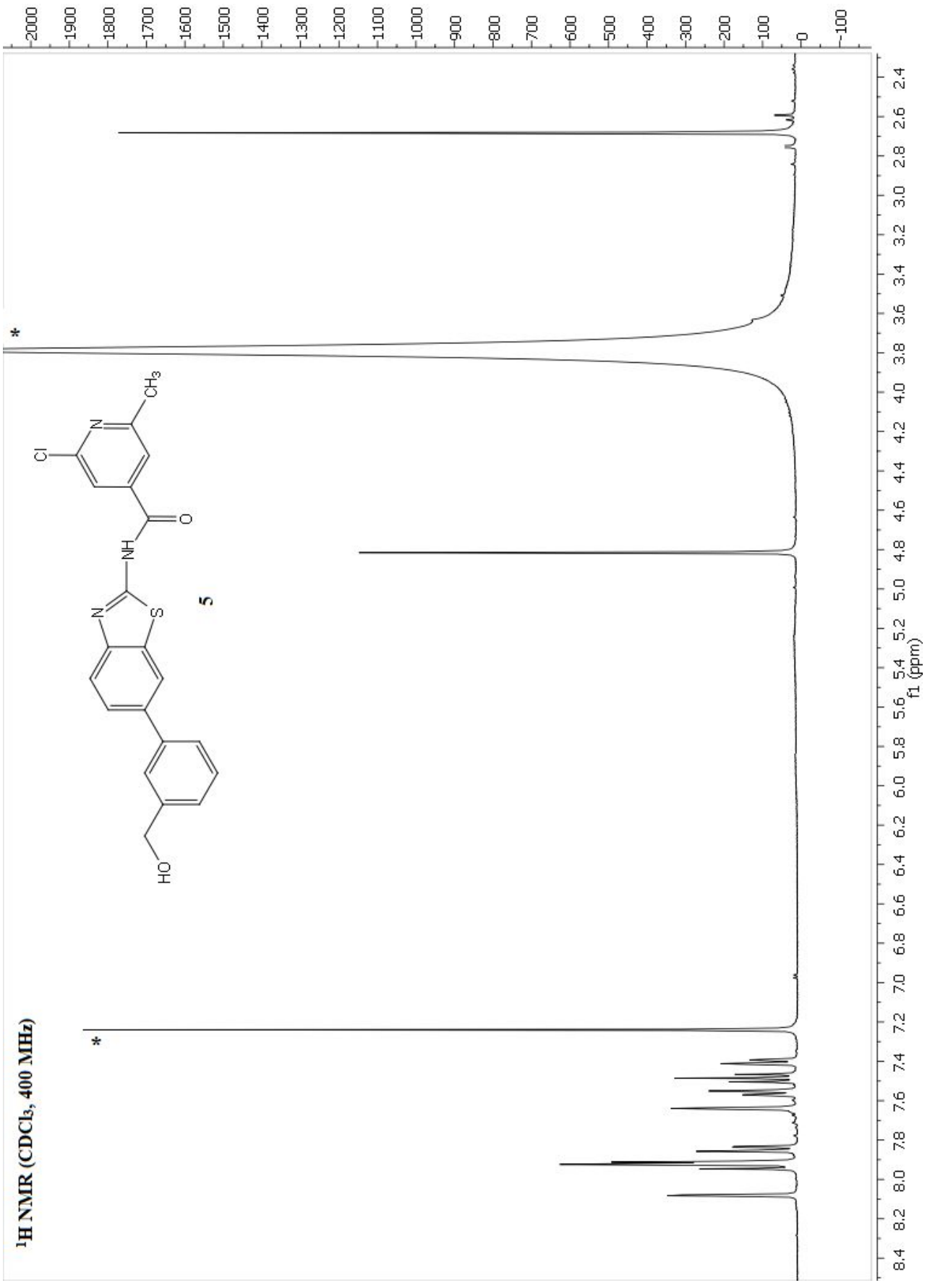

Figure S 23. Compound **5** ^{1}H NMR ($CDCl_3$, 400 MHz)

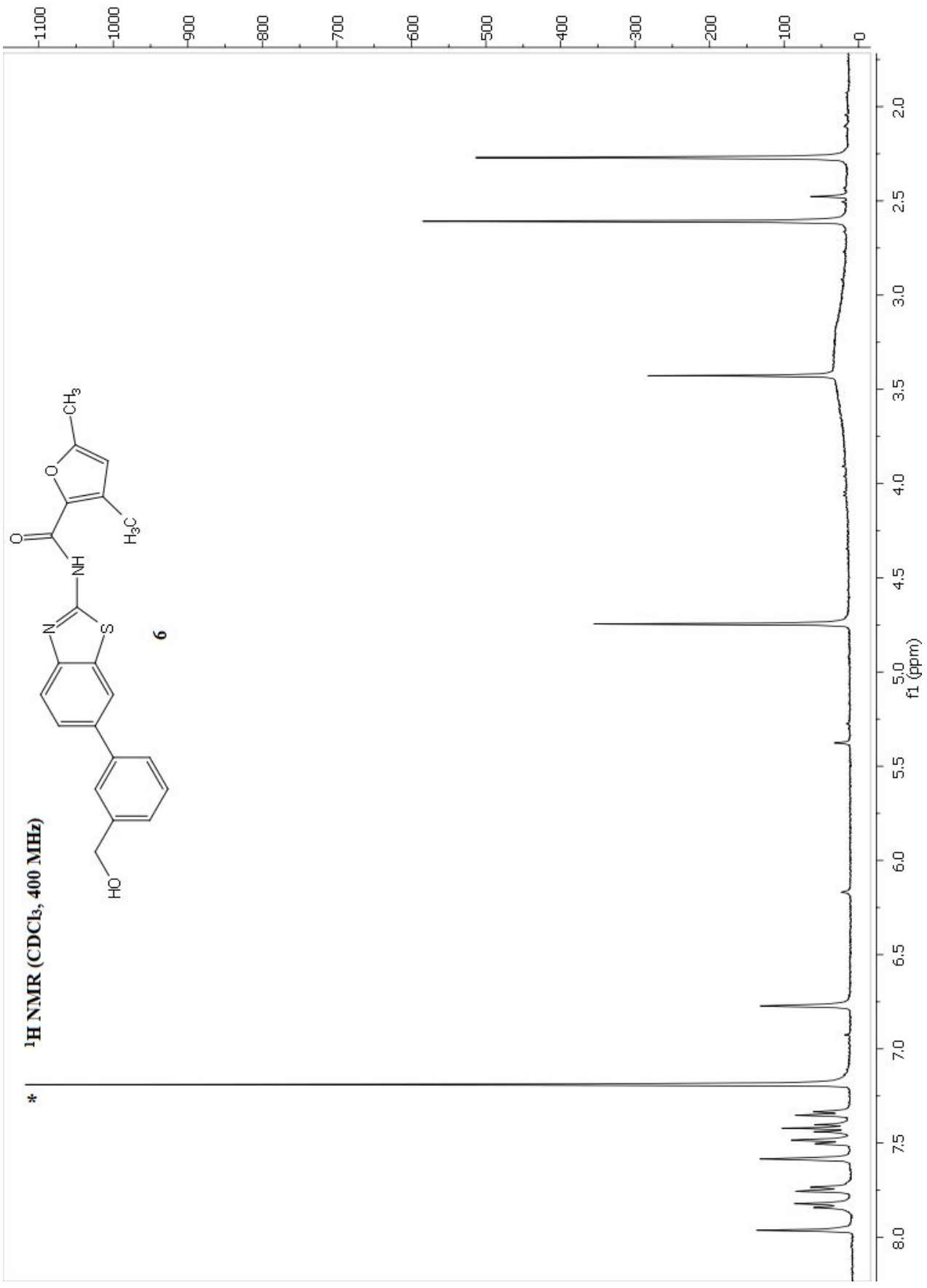

Figure S 24. Compound **6** ^{1}H NMR ($CDCl_3$, 400 MHz).

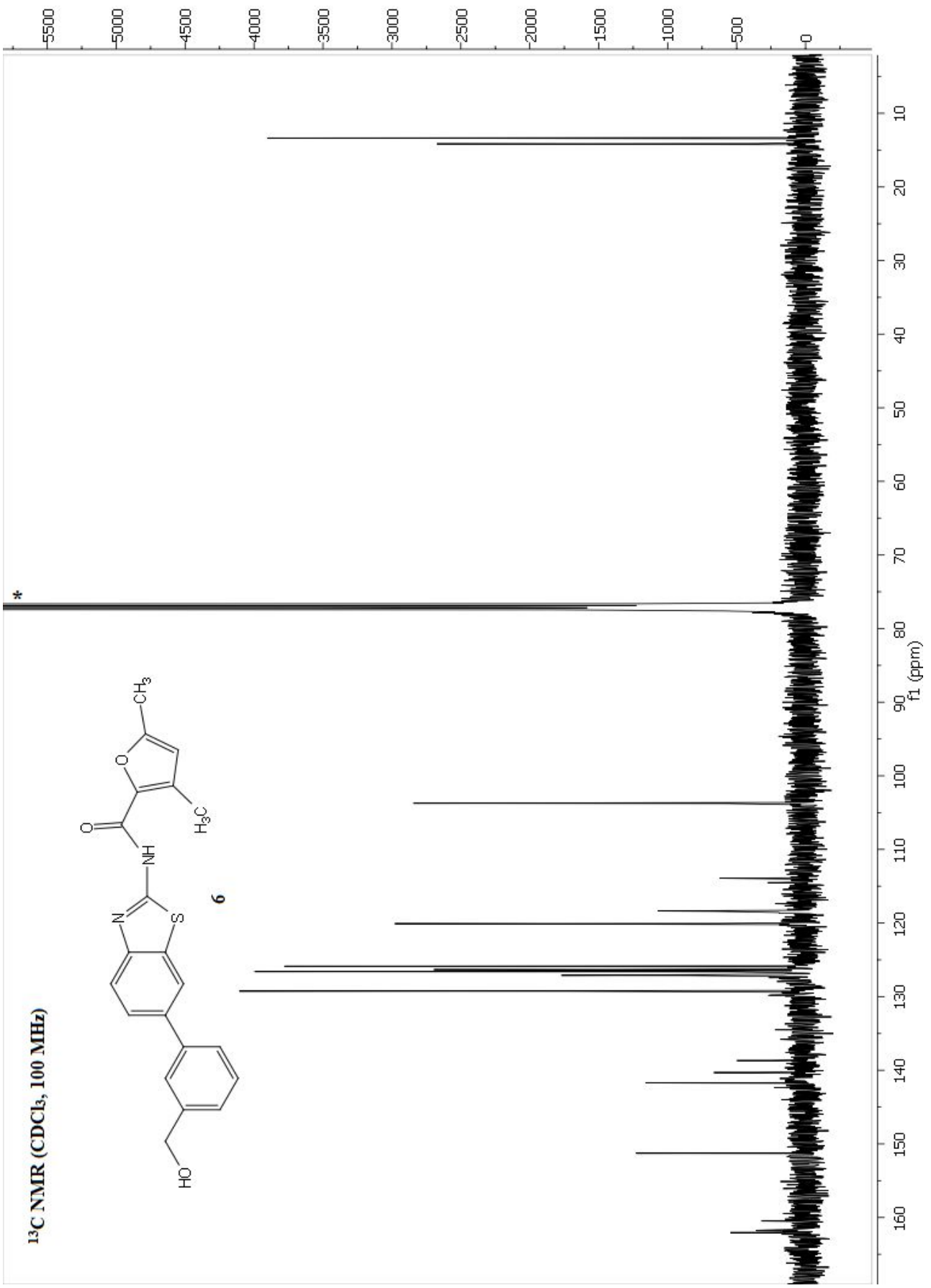

Figure S 25. Compound **6** ^{13}C NMR ($CDCl_3$, 100 MHz).

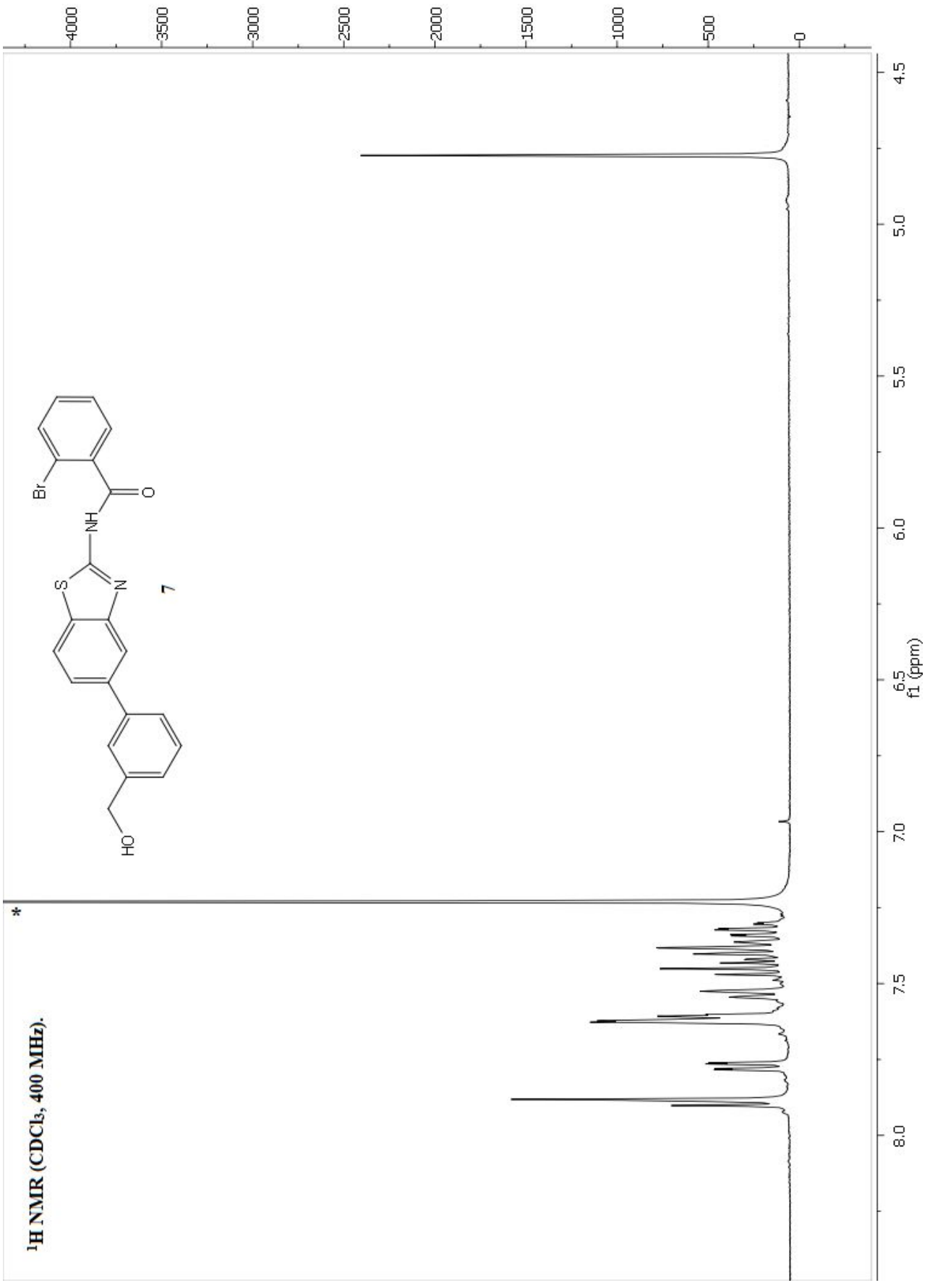

Figure S 26. Compound **7** ^{1}H NMR ($CDCl_3$, 400 MHz).

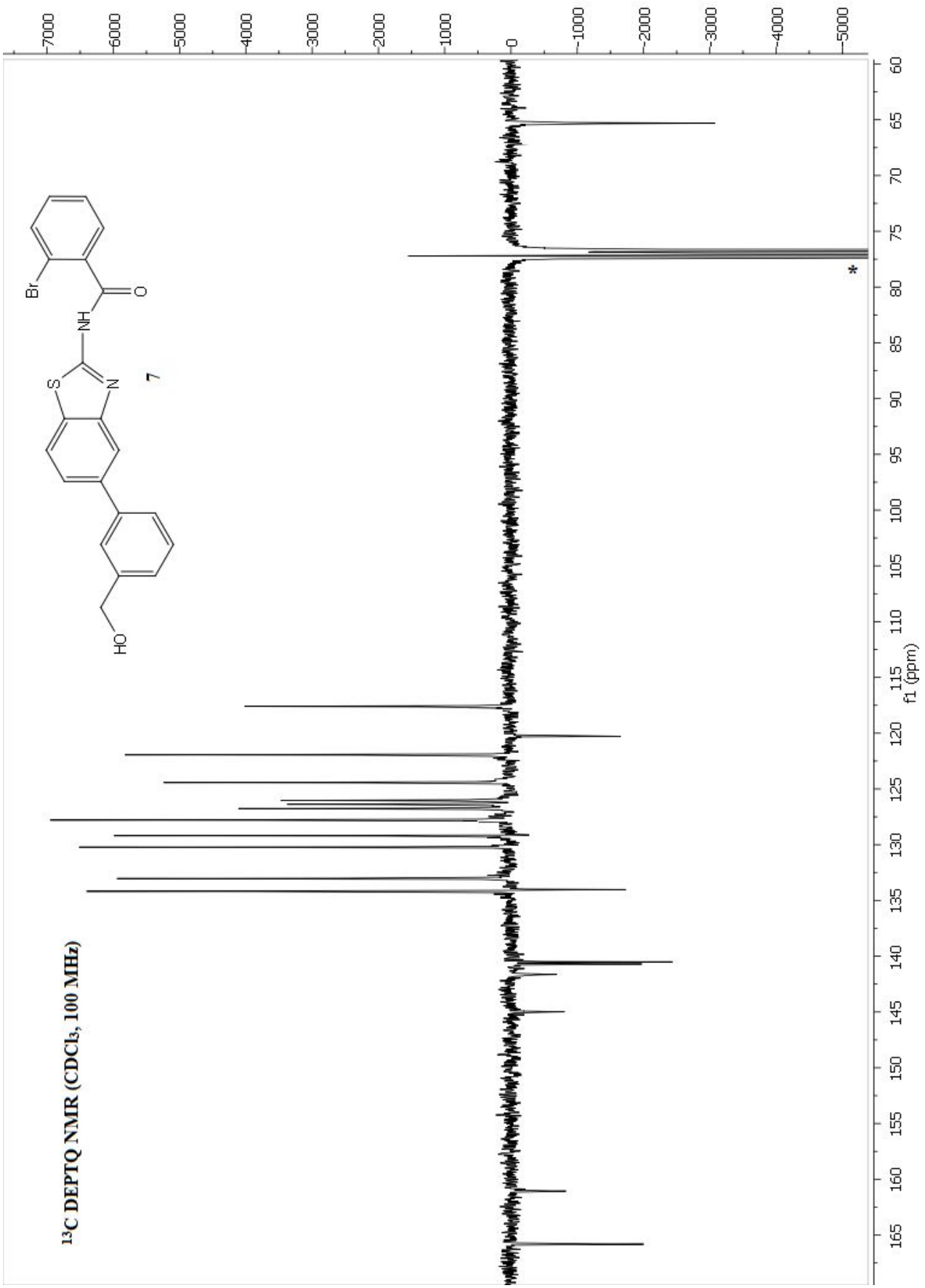

Figure S 27. Compound **7** ^{13}C DEPTQ NMR ($CDCl_3$, 100 MHz).

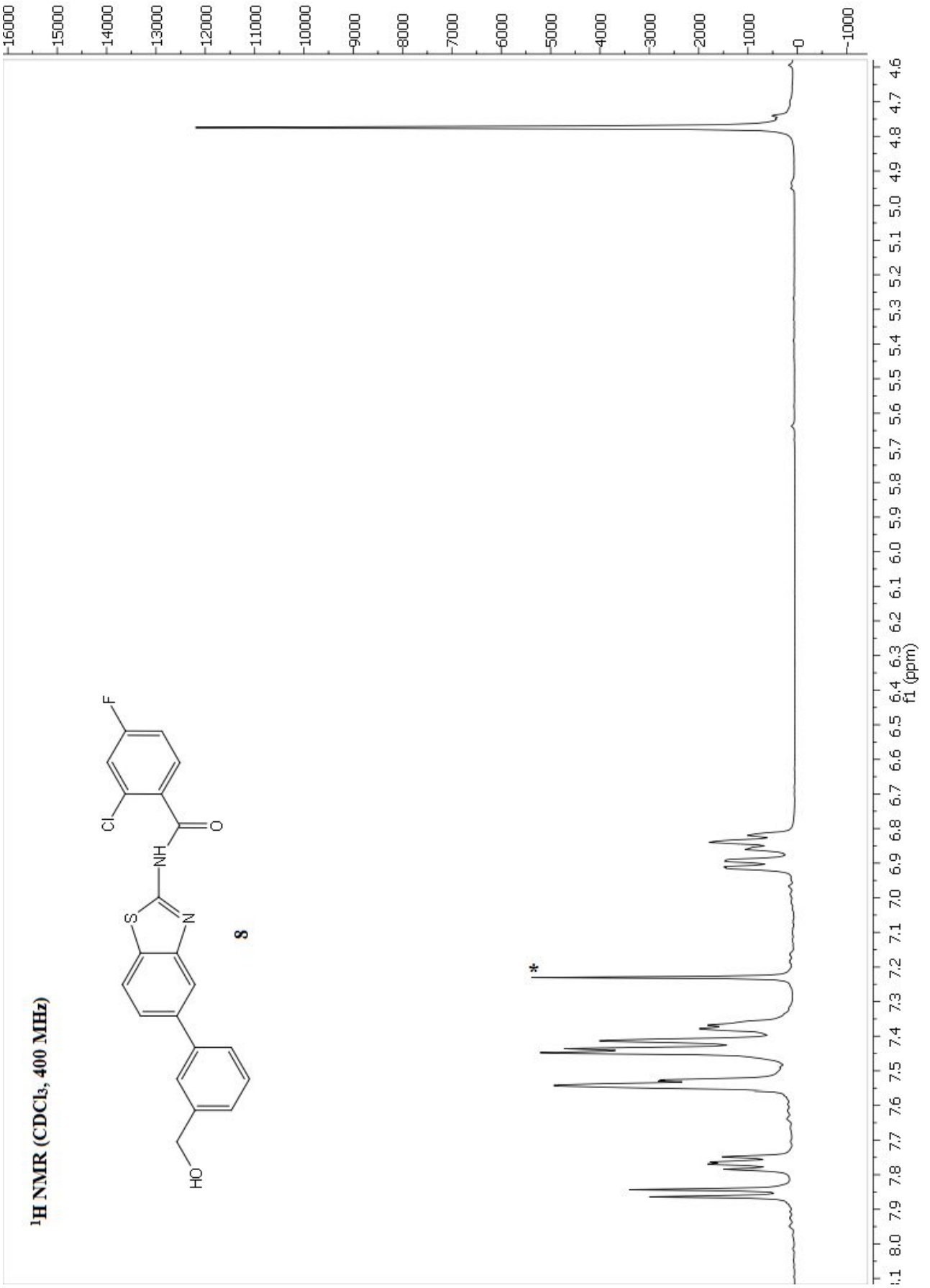

Figure S 28. Compound **8** ^{1}H NMR ($CDCl_3$, 400 MHz).

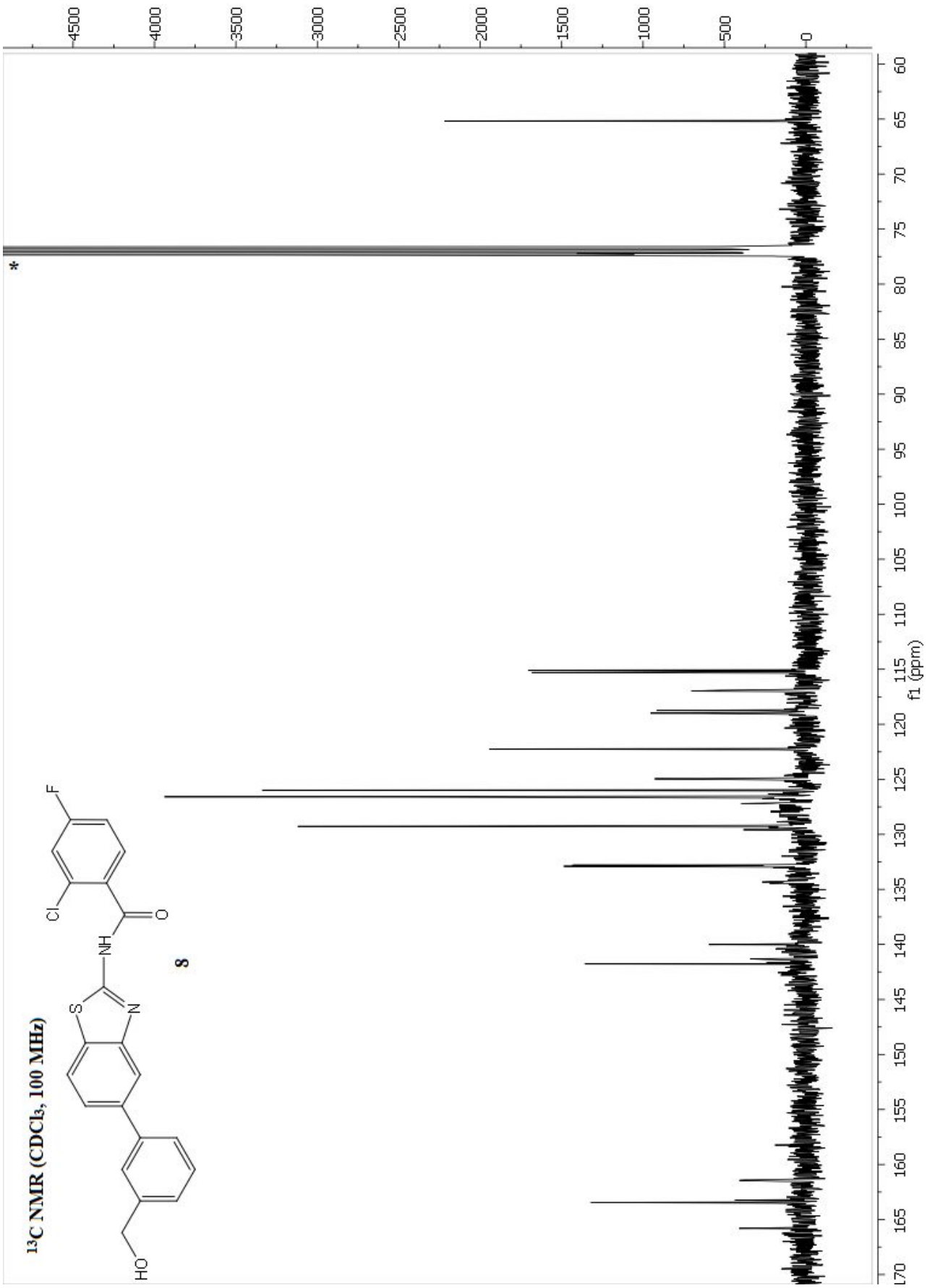

Figure S 29. Compound **8** ^{13}C NMR ($CDCl_3$, 100 MHz).

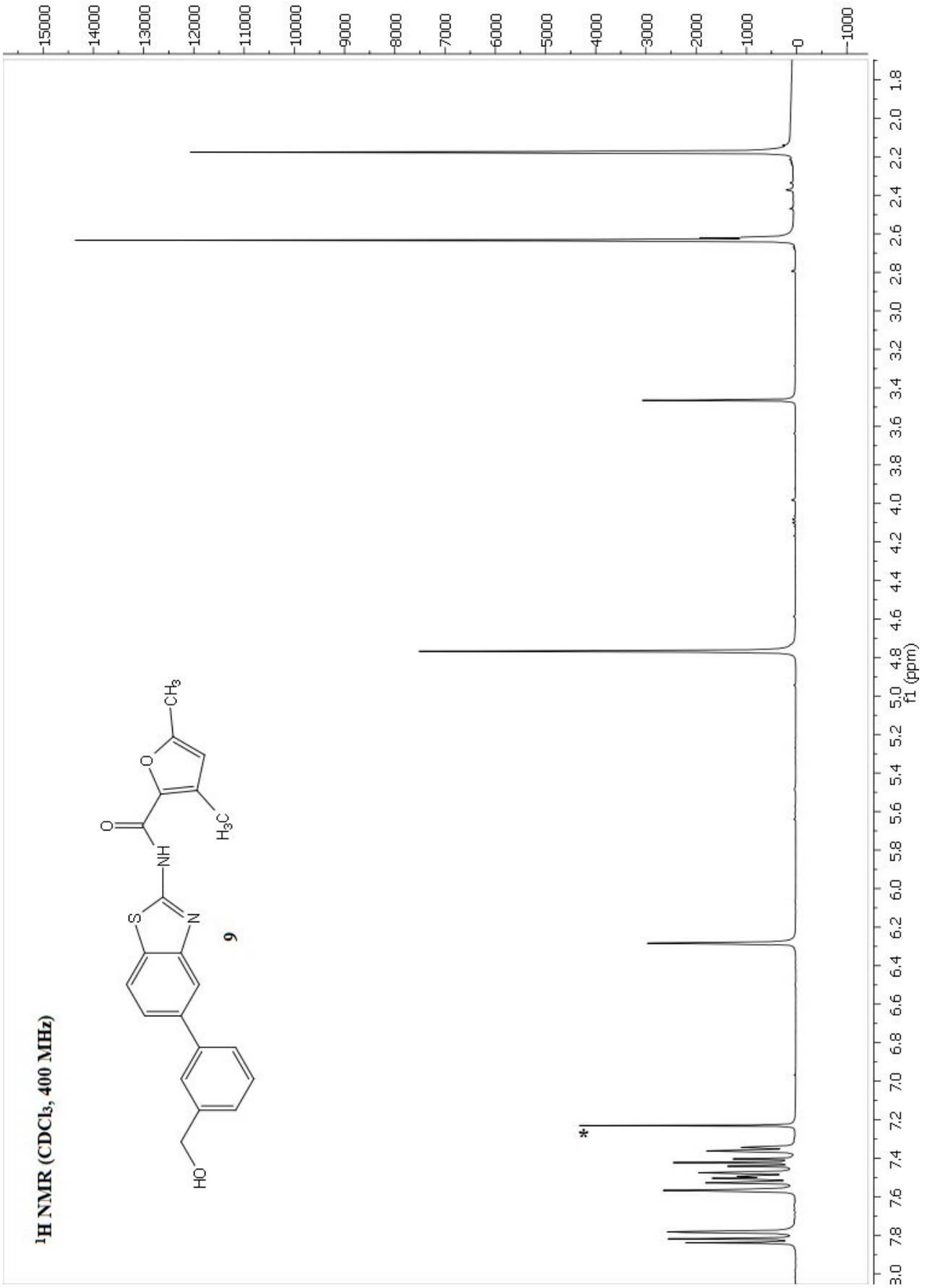

Figure S 30. Compound **9** ^{1}H NMR ($CDCl_3$, 400 MHz).

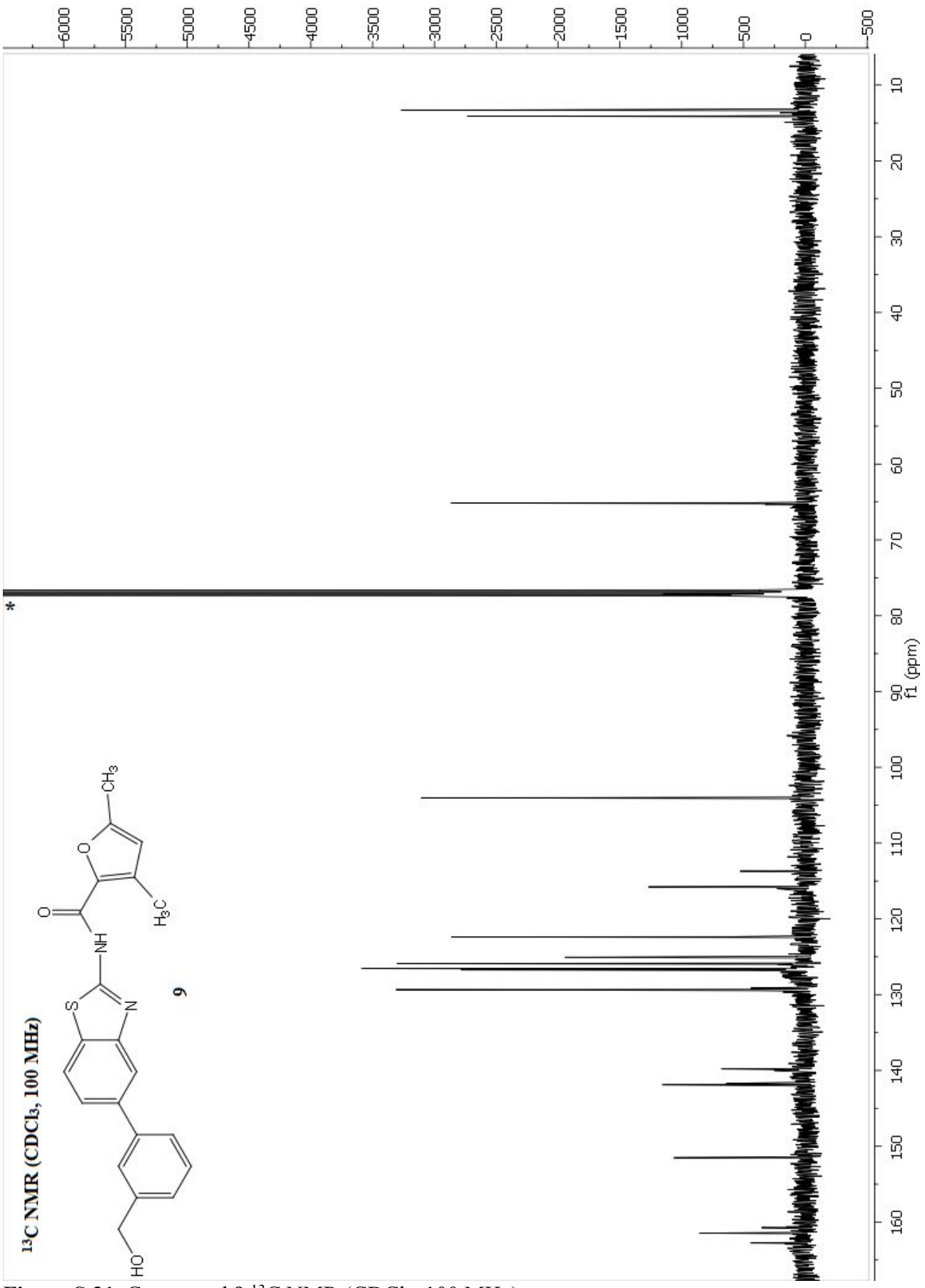

Figure S 31. Compound **9** ^{13}C NMR ($CDCl_3$, 100 MHz).

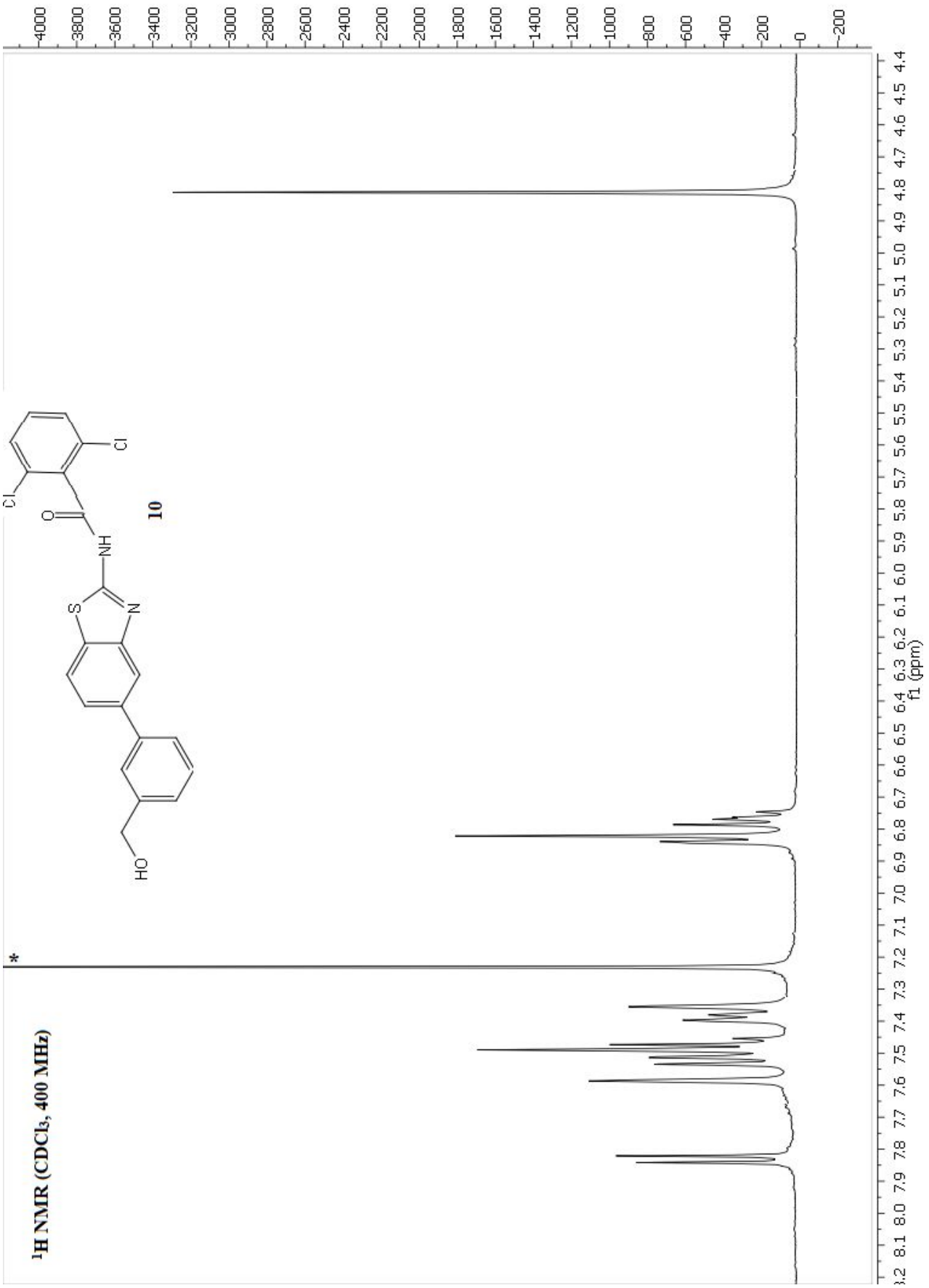

Figure S 32. Compound **10** ^{1}H NMR ($CDCl_3$, 400 MHz).

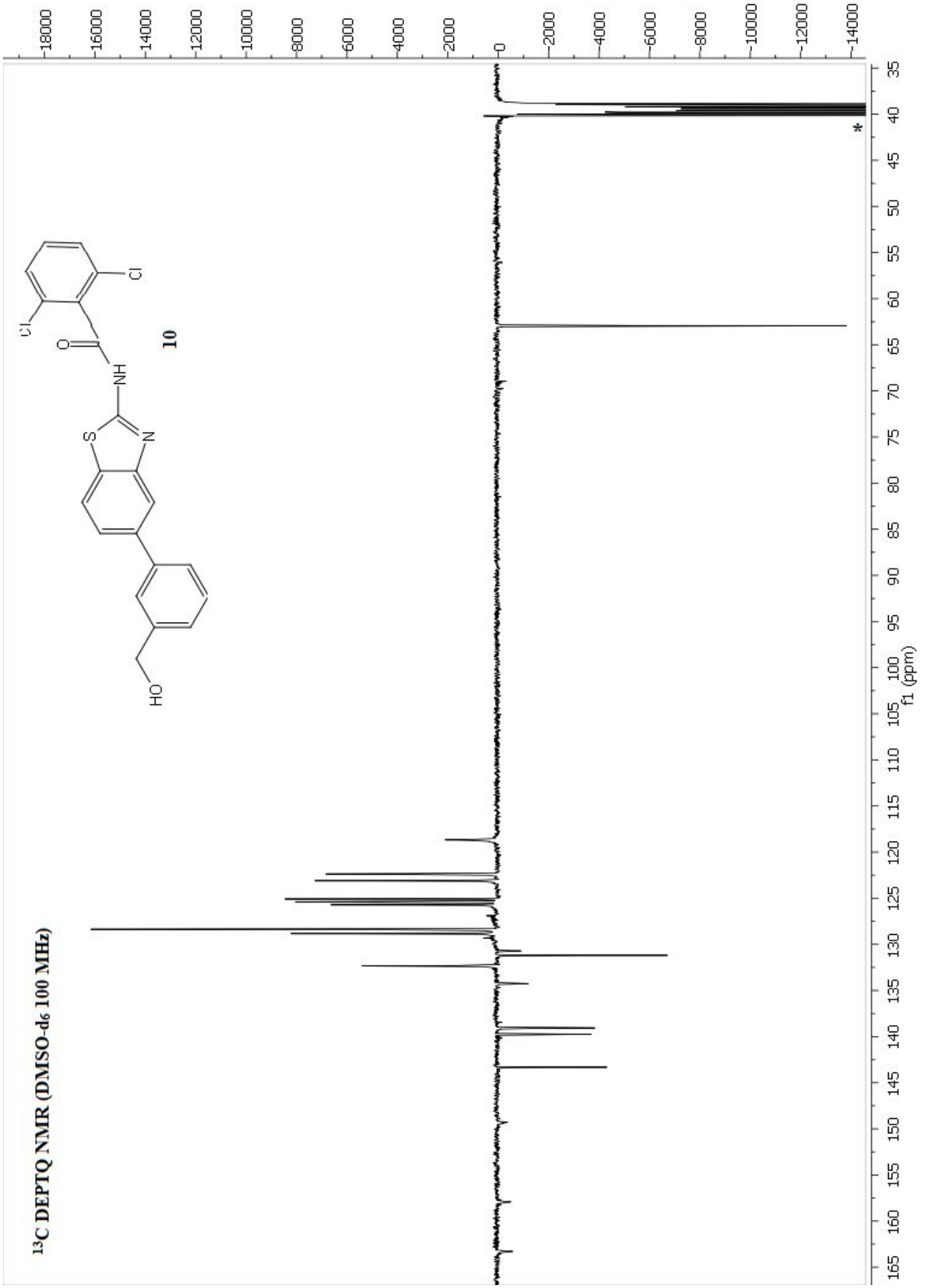

Figure S 33. Compound **10** ^{13}C DEPTQ NMR (DMSO-d_6 100 MHz).

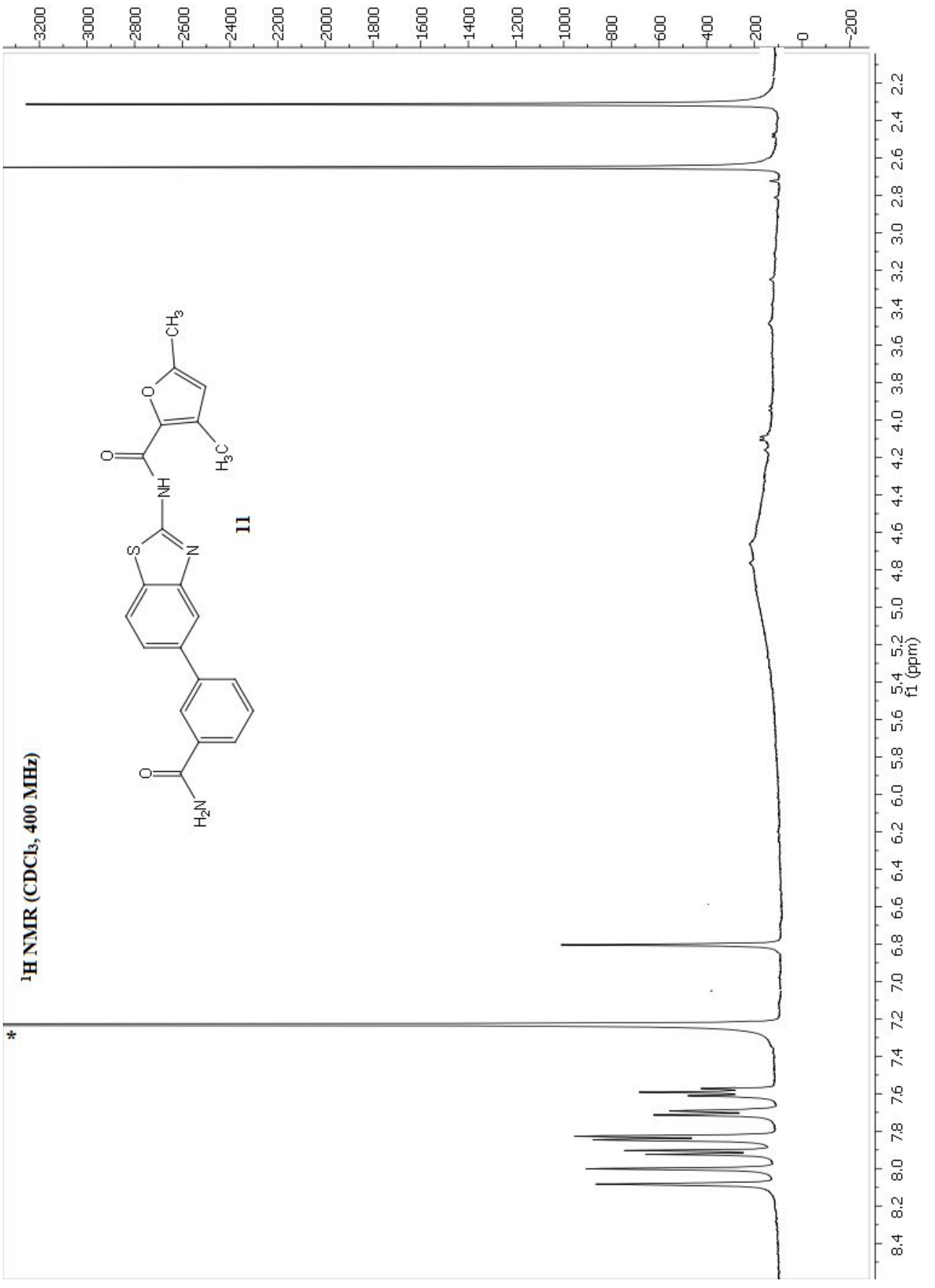

Figure S 34. Compound **11** ^{1}H NMR ($CDCl_3$, 400 MHz).

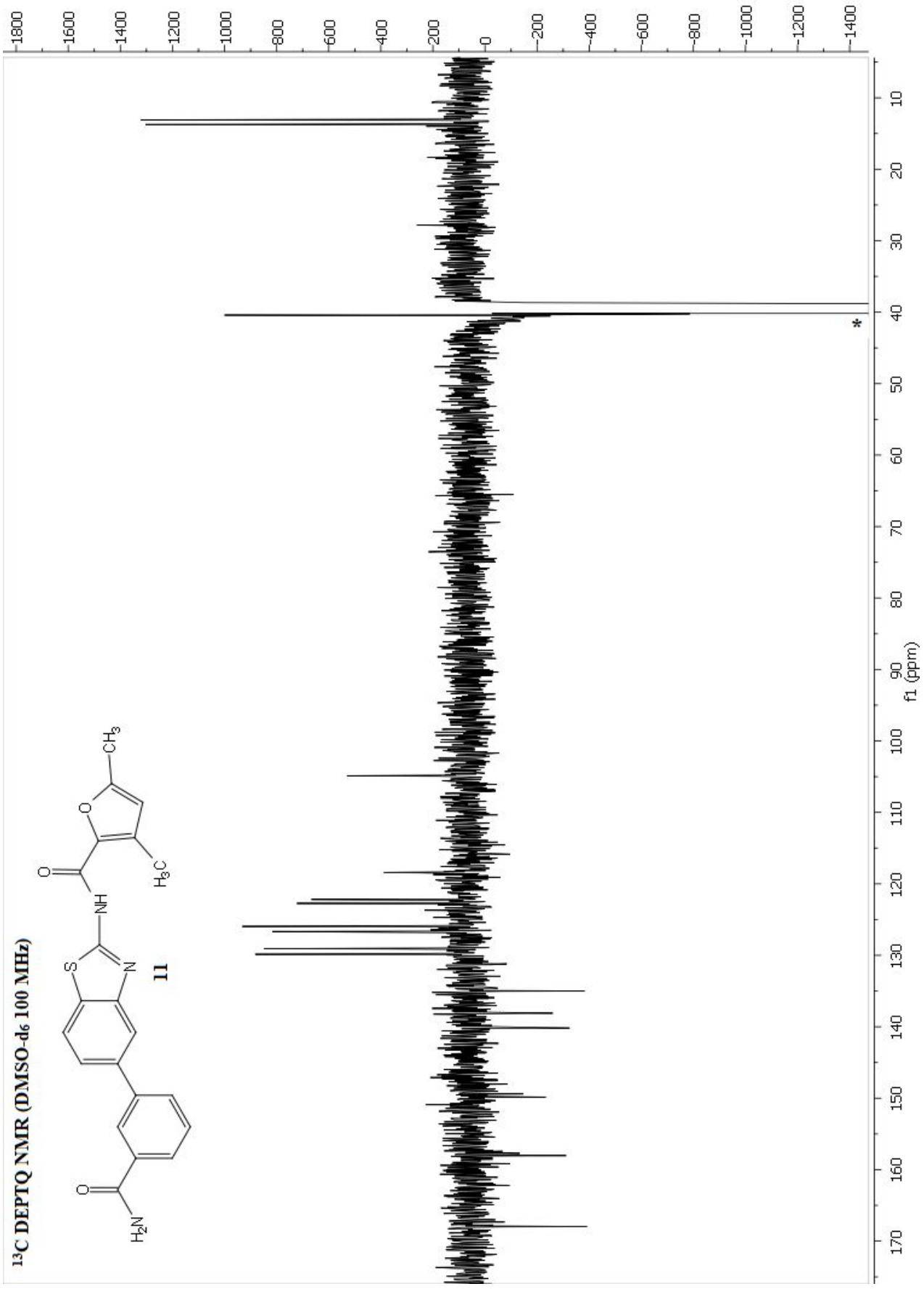

Figure S 35. Compound **11** ^{13}C DEPTQ NMR (DMSO-d_6 100 MHz).

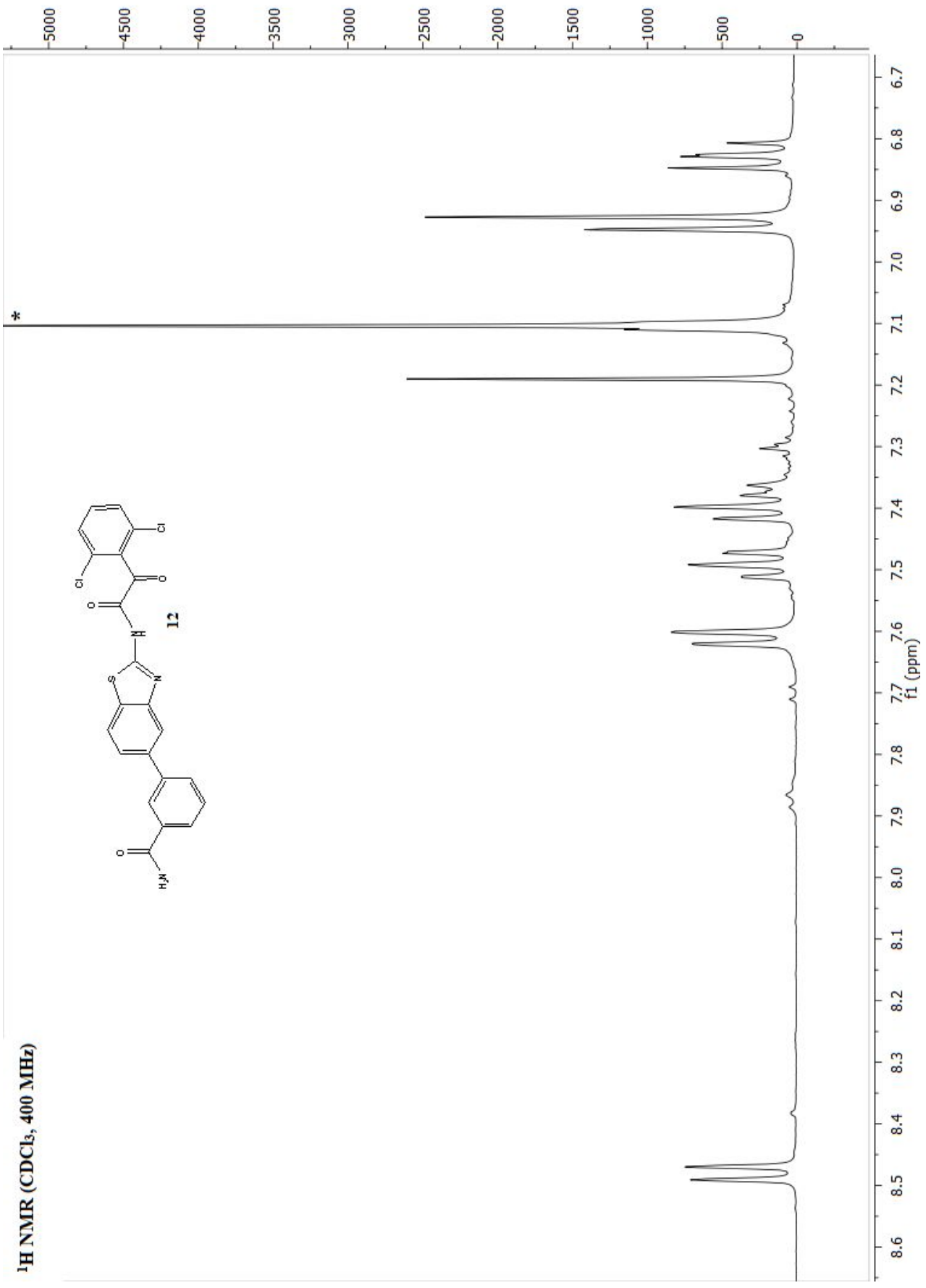

Figure S 36. Compound **12** ^{1}H NMR ($CDCl_3$, 400 MHz).

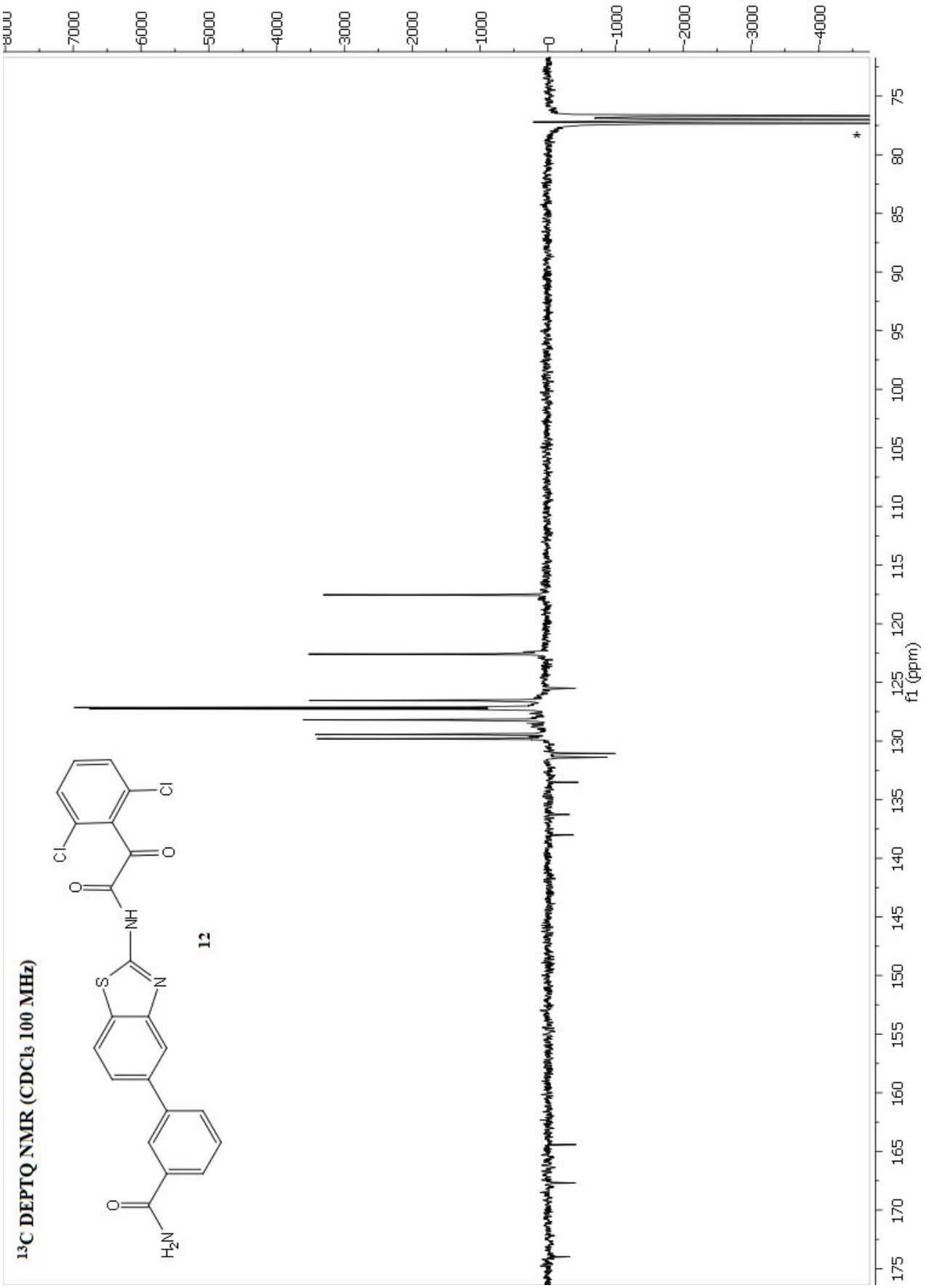

Figure S 37. Compound **12** ^{13}C DEPTQ NMR ($CDCl_3$ 100 MHz).

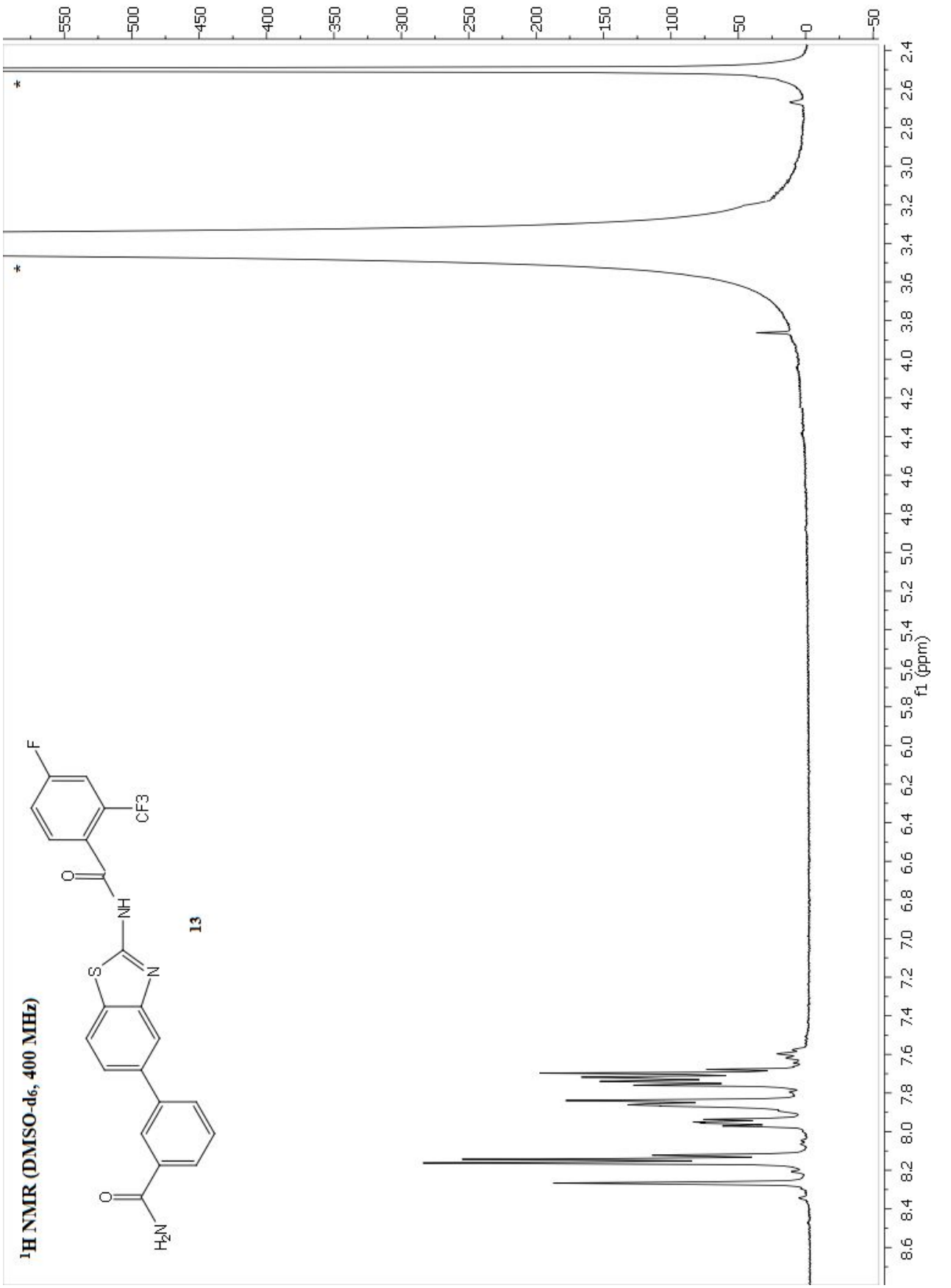

Figure S 38. Compound **13** ^{1}H NMR (DMSO-d$_6$, 400 MHz).

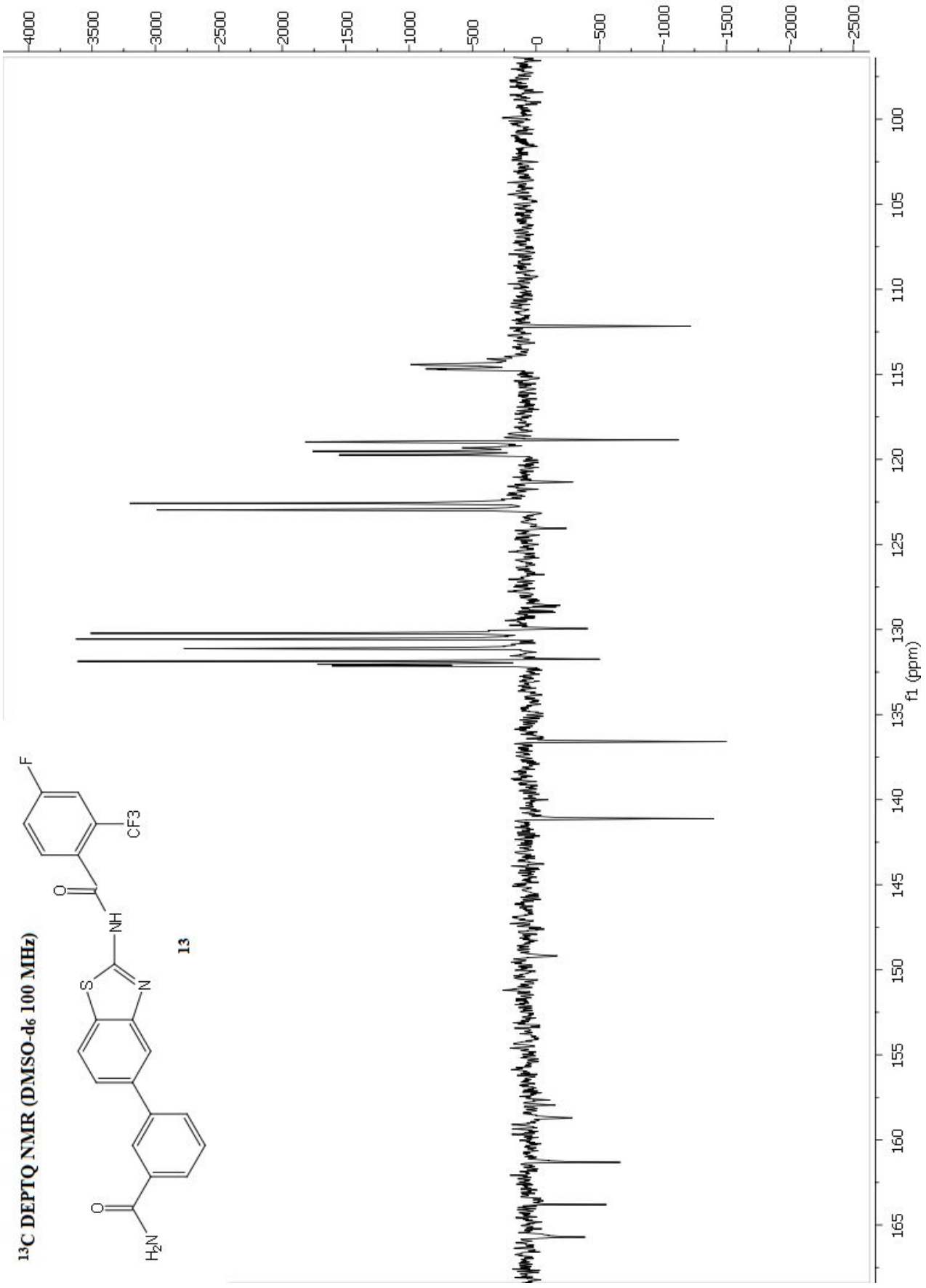

Figure S 39. Compound **13** ^{13}C DEPTQ NMR (DMSO-d_6 100 MHz).

Cell-free mPGES-1 activity assay

Microsomal prostaglandin E_2 synthase was obtained from microsomes of IL-1β-stimulated A549 cells. A549 cells were treated with IL-1β (1 ng/ml) for 48 h, and, thereafter, the cells were harvested, sonicated and the homogenate was submitted to differential centrifugation at 10,000×g for 10 min and 174,000×g for 1 h at 4 °C respectively. The microsomal fraction (pellet) was resuspended in 1 ml homogenization buffer (0.1 M potassium phosphate buffer, pH 7.4, 1 mM phenylmethanesulfonyl fluoride, 60 μg/mL soybean trypsin inhibitor, 1 μg/mL leupeptin, 2.5 mM glutathione, and 250 mM sucrose), the total protein concentration was determined, and microsomes were diluted in potassium phosphate buffer (0.1 M, pH 7.4) containing 2.5 mM glutathione.

Test compounds (or DMSO as a vehicle) were added, and preincubated for 15 min at 4 °C. Then, 20 μM of PGH_2 was added to initiate the reaction. After 1 min at 4 °C, 100 μl of a stop solution (40 mM $FeCl_2$, 80 mM citric acid, and 10 μM 11β-PGE_2) was added.

PGE_2 was extracted by RP-solid-phase extraction and analyzed by RP-UV-HPLC as described previously.[14]

Table S1 Cell-free mPGES-1 activity assay.

mPGES-1 residual activity tested at 10 μM ligand concentration and mPGES-1 IC_{50} values in cell free assay.

Compound	Residual activity (% at 10 μM)	IC_{50} ± SD (μM)
1		1.4±0.2
2	23.1	
3		0.7±0.1
4	92.3	
5	84.5	
6		2.6±0.1
7	43.0	
8	46.3	
9	55.2	

10	50.2	
11	85.8	
12	73.0	
13		1.7±0.2

Cell line

Human lung carcinoma A549 cells were purchased from Cell Application Inc., Sigma-Aldrich, Merck (Darmstadt, Germany) and maintained in DMEM supplemented with 10% heat-inactivated fetal bovine serum (Invitrogen, Carslbad, CA, USA) in 5% CO_2 humid atmosphere. To ensure logarithmic growth, the cells were subcultured every 2 days. The cell line was tested for Mycoplasma by PCR analysis.

Inhibition of cellular PGE_2 production

A549 cells were plated in DMEM with 10% FBS-medium at 10.000 cells/well in a 96-well plate. After overnight incubation, the cells were treated with 5 and 10 μM of **1**, **3**, **6**, **13** in DMEM plus 1% FBS and IL-1β (10 ng/ml) to upregulate the expression of PG synthases.

After 24 h, the amount of PGE_2 released in the supernatant was evaluated using a commercially available enzyme immunoassay kit (Prostaglandin E_2 EIA kit Monoclonal, Cayman Chemical). Cell viability was concomitantly evaluated using [3-4,5-dimethyldiazol-2-yl]-2,5-diphenyl tetrazolium bromide (MTT) reagent (Sigma-Aldrich). In brief, 20 μL of MTT (5 mg/mL in PBS) was added to each well, and cells were incubated for an additional 3 h at 37°C. The formazan crystals formed were dissolved in 100 μl of buffer containing 50% (v/v) *N*,*N*-dimethylformamide and 20% SDS (pH 4.5). The absorbance was measured at 570 nm with a Multiskan™ GO Microplate Spectrophotometer (Thermo Fisher Scientific, USA). The experiment was performed in triplicate.

Cell cycle progression analysis

A375 cells were treated with **1**, **3** and **13** (10, 20 or 30 μM) or DMSO for 48 or 72 h in DMEM

medium with 10% FBS. Compound concentrations were used close or above the IC_{50} values for inhibition of cellular PGE_2 biosynthesis. Cells were then harvested and incubated with propidium iodide (PI) solution (0.1% sodium citrate, 0.1% Triton X-100 and 50 mg/ml of PI) for 30 min at 4°C. For each sample, 10,000 events were recorded using FACScalibur flow cytometry (Becton Dickinson, San Josè, CA) and the proportion of cells in each cell cycle phase was calculated using ModFit LT software (BD). The necrotic/apoptotic cell fraction was quantified as the proportion of cells with hypodiploid DNA ($subG_0/G_1$ peak) using the CellQuest software (Becton Dickinson). Two independent experiments were performed, each in triplicate.

Statistical Analysis

All data represent the mean ± SD of at least three independent experiments performed in triplicate. The statistical significance of cell cycle distribution results was performed by two-way analysis of variance (ANOVA) with Bonferroni post-test analysis using GraphPad Prism 5 software. The P-value ≤ 0.05 was considered significant.

References

(1) Schrödinger Release 2017, Schrödinger, LLC, New York, NY, 2017.
(2) Protein Preparation Wizard workflow Schrödinger, LLC, New York, NY, 2017.
(3) CombiGlide Schrödinger, LLC, New York, NY, 2017.
(4) LigPrep Schrödinger, LLC, New York, NY, 2017.
(5) QikProp Schrödinger, LLC, New York, NY, 2017.
(6) Virtual Screening Workflow Schrödinger, LLC, New York, NY, 2017.
(7) Li, D.; Howe, N.; Dukkipati, A.; Shah, S. T.; Bax, B. D.; Edge, C.; Bridges, A.; Hardwicke, P.; Singh, O. M.; Giblin, G.; Pautsch, A.; Pfau, R.; Schnapp, G.; Wang, M.; Olieric, V.; Caffrey, M. Crystallizing Membrane Proteins in the Lipidic Mesophase. Experience with Human Prostaglandin E2 Synthase 1 and an Evolving Strategy. *Cryst. Growth Des.* **2014**, *14* (4), 2034-2047.
(8) Maestro version 10.2, Schrödinger, LLC, New York, NY **2017**.
(9) Glide Schrödinger, LLC, New York, NY, 2017.
(10) Friesner, R. A.; Banks, J. L.; Murphy, R. B.; Halgren, T. A.; Klicic, J. J.; Mainz, D. T.; Repasky, M. P.; Knoll, E. H.; Shelley, M.; Perry, J. K.; Shaw, D. E.; Francis, P.; Shenkin, P. S. Glide: a new approach for rapid, accurate docking and scoring. 1. Method and assessment of docking accuracy. *J. Med. Chem.* **2004**, *47* (7), 1739-1749.
(11) Halgren, T. A.; Murphy, R. B.; Friesner, R. A.; Beard, H. S.; Frye, L. L.; Pollard, W. T.; Banks, J. L. Glide: a new approach for rapid, accurate docking and scoring. 2. Enrichment factors in database screening. *J. Med. Chem.* **2004**, *47* (7), 1750-1759.
(12) Friesner, R. A.; Murphy, R. B.; Repasky, M. P.; Frye, L. L.; Greenwood, J. R.; Halgren, T.

A.; Sanschagrin, P. C.; Mainz, D. T. Extra precision glide: docking and scoring incorporating a model of hydrophobic enclosure for protein-ligand complexes. *J. Med. Chem.* **2006**, *49* (21), 6177-6196.
(13) Daina, A.; Michielin, O.; Zoete, V. SwissADME: a free web tool to evaluate pharmacokinetics, drug-likeness and medicinal chemistry friendliness of small molecules. *Sci. Rep.* **2017**, *7* 42717.
(14) Koeberle, A.; Siemoneit, U.; Buhring, U.; Northoff, H.; Laufer, S.; Albrecht, W.; Werz, O. Licofelone suppresses prostaglandin E2 formation by interference with the inducible microsomal prostaglandin E2 synthase-1. *J. Pharmacol. Exp. Ther.* **2008**, *326* (3), 975-982.